Pergamon

Deep-Sea Research II, Vol. 43, No. 7–8, pp. 1713–1744, 1996
Copyright © 1996 Elsevier Science Ltd
Printed in Great Britain. All rights reserved
PII: S0967-0645(96)00056-2
0967-0645/96 $15.00 + 0.00

Characterization of vertical mixing at a tidal-front on Georges Bank

JIRO YOSHIDA* and NEIL S. OAKEY†

(*Received* 15 *October* 1995; *in revised form* 1 *February* 1996; *accepted* 13 *May* 1996)

Abstract—Studies of mixing were done at the northern flank of Georges Bank in the summer and autumn of 1988. Two time-series of the evolution and intensity of microstructure were examined over a tidal period in the context of tidal forcing and the evolution of the density and velocity field at the site. From the CTD, ADCP and microstructure observations (EPSONDE) on Georges Bank, several interesting features of the mixing processes were found. High dissipation and diffusivity regions appear near the bottom of the Bank. Turbulence near the bottom is highest in intensity and reaches farthest from the bottom at peak tidal flow and diminishes in intensity and vertical extent as the flow decreases. The thickness of the bottom turbulent layer has its maximum value when the flow is strongest and the stratification is weakest. Characterization of the dissipation rate and turbulent diffusivities in respect to buoyancy frequency N, current shear S, Richardson Number R_i and $\varepsilon/\upsilon N^2$ was done. Dissipation and χ_T showed little dependence on shear or N^2 but decreased at larger R_i. χ_t was found to be higher in regions of higher N^2 and increased as $\varepsilon/\upsilon N^2$ increased. K_T, K_ρ and K_ν, were all highest near the bottom in excess of $10^{-2}\,m^2\,s^{-1}$ and decreased towards the surface. There was little suggestion of a dependence of mixing efficiency on S^2, R_i or $\varepsilon/\upsilon N^2$, but some indication that Γ decreases with decreasing N^2. Copyright © 1996 Elsevier Science Ltd

INTRODUCTION

Georges Bank on the northwestern Atlantic shelf to the east of Cape Cod and to the south of Nova Scotia, well known for its high biological productivity, is characterized by a pronounced tidal-mixing front. This front extends around the bank near the 60 m isobath during the spring–autumn period. Previous investigations indicate the importance of the variability of the front to this high productivity (e.g. Loder and Platt, 1985; Horne *et al.*, 1989). Riley (1982) also pointed out that high vertical mixing rates over the Bank front could be responsible for enhanced regeneration of nutrients. Nevertheless, the precise nature of the mixing processes is still not clear.

An extensive field study of mixing processes at this tidal mixing front was undertaken in the Bedford Institute's 1988 Georges Bank Frontal study. An overview of some of the results of this study is given in Loder *et al.* (1993) and Fig. 1 from that paper is used here as a reference for the study area. The area is dominated by a strong tidal front determined largely by temperature. Intensive observations at each of the four sites shown on the figure were obtained from a CTD, an acoustic doppler current profiler, and in particular the microstructure profiler, EPSONDE. Details of the hydrography and currents are discussed in detail in Loder *et al.* (1992). They confirm previous observations of strong

* Department of Marine Science and Technology, Tokyo University of Fisheries, 4–5–7 Konan, Minato-ku, Tokyo 108, Japan.

† Ocean Sciences Division, Department of Fisheries and Oceans, Bedford Institute of Oceanography, P.O. Box 1006, Dartmouth, Nova Scotia, Canada B2Y 4A2.

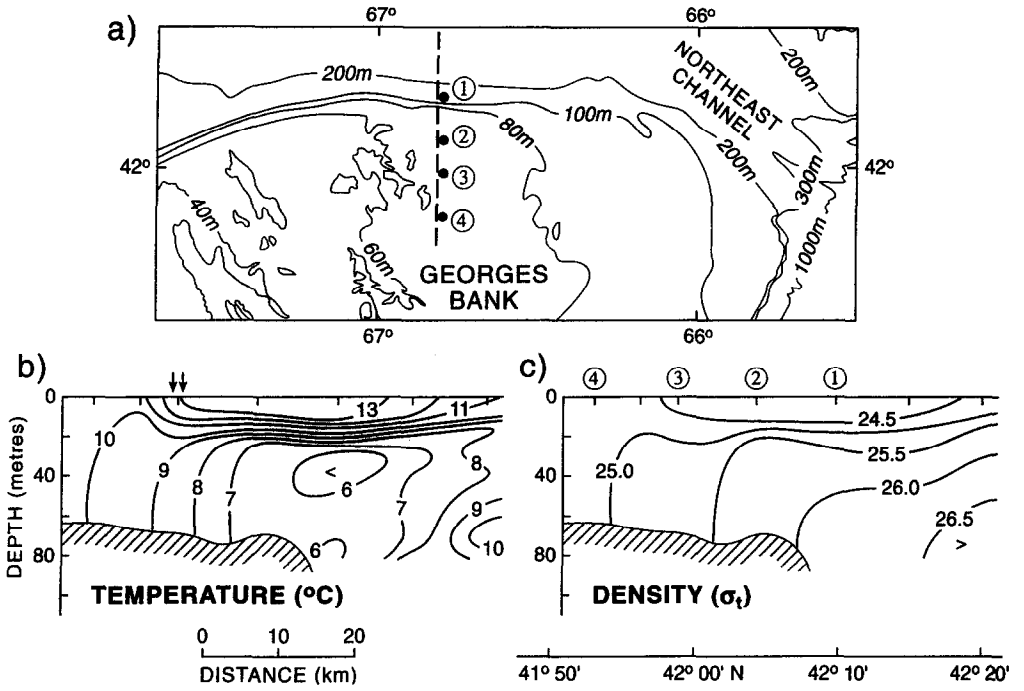

Fig. 1. The Georges Bank Frontal study area is shown (a) with the four principal study sites on a north–south line crossing the bank edge at 66°W. The mean temperature (b) and density fields (c) are shown as contour plots in relation to these four sites. Site 2 at the strongest frontal expression is discussed in this paper.

tidal and residual currents, internal tide and tidal front, but also describe a richness of internal wave structure, an internal hydraulic jump and solitary waves generated at the bank edge moving into the frontal zone. As we shall see later, the complexity of this region makes it difficult to characterize the turbulent mixing processes. In a previous study in 1985, Horne *et al.* (1995) made similar studies to those reported in this paper. Their microstructure measurements, nevertheless, did not go to the bottom and did not have the concurrent ADCP data.

It is the purpose of the present paper to explore the relationships between various turbulence parameters commonly used to quantify the intensity of turbulence and mixing rates. A major difficulty in merging data from the microstructure profiler (which goes to the bottom) and the CTD and ADCP profilers (which do not go to the bottom) is that a concomitant set of data from all sources largely ignores the lowest 5–8 m of the water column. We are therefore unable to satisfactorily quantify the bottom boundary layer thickness and its variability.

We focus our attention on mixing processes at Site 2, which is on the bank and likely to be the site most temporally affected by velocity and density changes as a result of the tide. Because the front is tidally forced, it is advected on and off the bank past the measurement site by the barotropic tide, providing a wide range of currents over the tidal period and at the same time a varying mixing environinent as the density and density gradient change. The frontal expression has extreme positions separated by 10–15 km. Previous studies of turbulence in shallow seas where tidal forcing is high (Dewey and Crawford, 1988; Loder *et*

al., 1992; Horne *et al.*, 1995) lead one to expect that in our study area a major factor in determining the intensity of turbulence should be the shear flow, particularly in the bottom boundary layer. One might expect mixing to be strongest when the tidal flow is greatest and the bottom boundary layer shear the largest. It also should be damped as the density gradient increases. Site 2 was chosen for the current investigation because it is characterized by strong changes in velocity, velocity shear and density gradient. In the upper water column the situation may be much more complicated with internal waves or solitons contributing to mixing. Near the surface, energy from the wind field and stratification from surface heat flux will be an additional complication. We will show data to contrast mixing at times reflecting stronger off-bank and on-bank flow periods to those periods when the currents are low. We will explore in the paper the way in which mixing is dependent on factors such as shear and density gradient and try to characterize mixing rates (e.g. vertical diffusivity) at this site in terms of the larger scale forcing quantities. This may provide a way in which these sub-grid-scale processes may be more easily and correctly incorporated into models.

INSTRUMENTATION AND DATA ANALYSIS

CTD measurements

A Guildline model 8715 S/N 53100 CTD (Conductivity, Temperature and Depth Profiler) was used to observe temperature, salinity and density structure on Georges Bank. CTD observations were conducted as near to the bottom as possible (typically 5 m) and at approximately 1 h intervals at both tidal-long series at Site 2. Conductivity, temperature and pressure data were sampled at 25 Hz. Abnormal spikes in the data were removed by using a median filter technique. Data were averaged and decimated to approximately 1 m vertical depth bins. On each CTD cast, salinity samples taken from the deepest bottle were measured using a Guildline AUTOSAL salinometer in the laboratory to calibrate CTD salinity data. The pressure sensor was calibrated using a dead weight pressure standard before and after the cruise.

ADCP measurements

Current speed and direction measurements were obtained using a ship-mounted Ametek Straza 300-kHz ADCP (Acoustic Doppler Current Profiler) with a repetition period of 3 s and a pulse length, resulting in velocity components averaged vertically in 3.1 m bins. The water velocity profile was calculated from the relative water velocity and the bottom-tracked velocity. The data from good acoustic returns were averaged over 10 min. Cochrane (1985) estimated the noise associated with the ADCP in this configuration from the single ping standard deviation divided by the square root of the number of pings in a 10 min average. This gives a 0.015 m s^{-1} standard error for the relative water velocity and 0.002 m s^{-1} for the bottom tracked velocity. Values of $S^2 < 10^{-5}$ thus may be affected by instrument noise. Details of data processing for the ADCP in the context of other current measurements are given in Loder *et al.* (1990).

EPSONDE measurements

Microstructure measurements were conducted by using EPSONDE (Oakey, 1988b), a

tethered free-fall instrument, falling at a speed of about 0.8 m s^{-1}. A strain gage pressure transducer and thermistor measure pressure and temperature sampled at 32 Hz. Temperature microstructure was observed with a fast thermistor sampled at 32 Hz, and the differentiated signal from this sensor was also sampled at 128 Hz. From this differentiated signal, temperature gradients were calculated by assuming a frozen field and invoking Taylor's hypothesis and the instruments measured drop velocity. Shear probes (Osborn and Crawford, 1980) were used to measure velocity microstructure. The turbulent velocity shear data were obtained by passing the velocity signal from the probe through an electronic differentiator and sampling at 256 Hz. The data were analyzed in segments of 2 s (64 samples for pressure and temperature data, 512 for microstructure data), which is equivalent to approximately 1.6 m blocks. For each segment, average depth, temperature and temperature gradient were calculated. Microstructure data were analyzed spectrally to obtain variances of temperature gradient and shear after correcting the signals for sensor and electronic transfer functions and removal of noises and spikes. From this data set, microstructure quantities, such as energy dissipation rate and turbulent eddy diffusivities, were calculated by using the following equations.

Although most of the definitions below are in previous papers, it is convenient to give them here for completeness. The turbulent kinetic energy equation (simplified by assuming isotropy and homogeneity) is given as

$$\frac{\mathrm{d}}{\mathrm{d}t}\left(\frac{1}{2}\overline{q^2}\right) = -\overline{u'w'}\frac{\partial \bar{U}}{\partial z} - \varepsilon - g\frac{\overline{\rho'w'}}{\rho}, \tag{1}$$

where $\frac{\mathrm{d}}{\mathrm{d}t}\left(\frac{1}{2}\overline{q^2}\right)$ is the rate of change of mean turbulent kinetic energy, $-\overline{u'w'}\frac{\partial \bar{U}}{\partial z}$ is the production of turbulent kinetic energy by the work of Reynolds stress against vertical mean shear, ε is the dissipation of turbulent kinetic energy, and $-g\frac{\overline{\rho'w'}}{\rho}$ is the production of potential energy by the buoyancy force. Here, the overbar denotes the ensemble average. u' and w' are horizontal and vertical fluctuation velocities, respectively. ρ is density and ρ' is the density fluctuation.

The energy dissipation ε is given by (Osborn, 1980)

$$\varepsilon = 7.5\upsilon\overline{\left(\frac{\partial u'}{\partial z}\right)^2}\ \mathrm{W\ kg^{-1}} \tag{2}$$

where $\overline{\left(\frac{\partial u'}{\partial z}\right)^2}$ is the variance in the vertical gradient of turbulent fluctuation in the x-direction (perpendicular to the z-axis upward). Here, isotropic turbulence is assumed. υ is the kinematic viscosity ($\upsilon = 1.3 \times 10^{-6}\ \mathrm{m^2\ s^{-1}}$).

The vertical diffusivity of density K_ρ is defined as

$$K_\rho \frac{\partial \rho}{\partial z} = -\overline{\rho'w'}. \tag{3}$$

The flux Richardson number, R_f, defined as the ratio of the production of potential energy to that of kinetic energy (see Equation (1)), is

$$R_f = \frac{g\overline{\rho'w'}}{-\rho\overline{u'w'}\frac{\partial \bar{U}}{\partial z}}. \tag{4}$$

If the change of mean turbulent kinetic energy is small ($\frac{\mathrm{d}}{\mathrm{d}t} \approx 0$), K_ρ is given by using (1), (3) and (4) as

$$K_\rho = \Gamma \frac{\varepsilon}{N^2} = \frac{R_f}{1 - R_f} \frac{\varepsilon}{N^2} \text{ m}^2 \text{ s}^{-1}, \tag{5}$$

where Γ is a parameter referred to often as the mixing efficiency. The value of Γ in terms of critical value of the flux Richardson number, R_f, is less than 0.25 as discussed in Osborn (1980), and for this paper we use a value of $\Gamma = 0.25$ (Oakey, 1985). N is the buoyancy frequency ($N^2 = \frac{g}{\rho}\frac{\partial \rho}{\partial z}$). This formulation will not be valid if there is no stratification. There does not need to be stratification for there to be turbulence, but there does need to be stratification for there to be mixing (or more generally a property gradient).

The structure of the bottom boundary layer turbulence (in the unstratified case) can be expressed as the balance between production of turbulent kinetic energy by Reynolds stress acting on the mean shear and dissipation by simplifying the TKE equation for unstratified flow (Hinze, 1975). This leads to the definition of the vertical diffusivity of momentum K_v,

$$K_v \frac{\partial \bar{U}}{\partial z} = -\overline{u'w'}. \tag{6}$$

If the buoyancy production of potential energy is neglected and ($\frac{d}{dt} \approx 0$) is assumed in Equation (1), then K_v is given by

$$K_v = \frac{\varepsilon}{\left(\frac{\partial \bar{U}}{\partial z}\right)^2} \text{ m}^2 \text{ s}^{-1}, \tag{7}$$

where $\left(\frac{\partial \bar{U}}{\partial z}\right)^2$ is the vertical mean shear squared defined as $S^2 = \left(\frac{\partial \bar{U}}{\partial z}\right)^2 = \left(\frac{\partial \bar{u}}{\partial z}\right)^2 + \left(\frac{\partial \bar{v}}{\partial z}\right)^2$. Here, $\bar{u}$ is the north–south component and $\bar{v}$ is the east–west component of current velocity measured by ADCP. Here, velocity shear is calculated from upper and lower adjacent velocity points. For example, velocity shear for the depth i, $\left(\frac{\partial \bar{u}}{\partial z}\right)_i$ is calculated as

$$\left(\frac{\partial \bar{u}}{\partial z}\right)_i = (\overline{u_{i-1}} - \overline{u_{i+1}})/\Delta z (\Delta z = 6.2 \text{ m}). \tag{8}$$

The turbulent temperature fluctuation equation is defined analogous to Equation (1) as

$$\frac{d}{dt}\overline{(T')^2} = -\overline{w'T'}\frac{\partial \bar{T}}{\partial z} - \frac{1}{2}\chi_T, \tag{9}$$

where $\frac{d}{dt}\overline{(T')^2}$ is the rate of change of temperature variance, $-\overline{w'T'}\frac{\partial \bar{T}}{\partial z}$ is the production of temperature variance by buoyancy flux, and $\frac{1}{2}\chi_T$ is the dissipation of temperature gradient variance by molecular diffusion.

The dissipation of temperature gradient χ_T is given by

$$\chi_T = 6D\overline{\left(\frac{\partial T'}{\partial z}\right)^2} \text{ °C}^2 \text{ s}^{-1}, \tag{10}$$

where isotropy is also assumed, and D is the molecular diffusivity of heat ($1.4 \times 10^{-7} \text{ m}^2 \text{ s}^{-1}$). The vertical diffusivity of heat K_T is defined as

$$K_T \frac{\partial \bar{T}}{\partial z} = -\overline{w'T'}. \tag{11}$$

If the rate of change of temperature variance is small ($\frac{d}{dt} \approx 0$), then from Equations (9), (10) and (11) we have an expression for K_T as

$$K_T = 3D\frac{\overline{(\partial T'/\partial z)^2}}{(\partial \bar{T}/\partial z)^2} = 3DC_x \text{ m}^2 \text{ s}^{-1}, \tag{12}$$

where C_x is the Cox number (Osborn and Cox, 1972).

EPSONDE was profiled repeatedly (typically eight times) down to the bottom within a 30–40 min period at approximately 1 h intervals (called a BURST). Temperature, pressure and microstructure data from each BURST were averaged in bins of 3.1 m (to correspond to the ADCP data) to give hourly averaged EPSONDE data profiles. To examine more closely the dependence of turbulent intensity on large-scale shear, EPSONDE data also were averaged over 10 min centred around the ADCP observation time to give 10 min averaged data. Along with this, the velocity shear was calculated from ADCP data to obtain K_ν and the Richardson number. The Richardson number is defined by

$$R_i \frac{N^2}{\left(\frac{\partial \bar{U}}{\partial z}\right)^2} = \frac{N^2}{S^2}. \tag{13}$$

Previous investigations (e.g. Turner, 1973) indicate that sheared stratified flow becomes unstable when R_i becomes lower than critical number 0.25. It might be expected that the fluid layer becomes more turbulent and mixing enhanced at lower Richardson number.

To calculate K_ρ and R_i, the buoyancy frequency for the hourly averaged data was calculated from the CTD profile closest in time to the EPSONDE station since EPSONDE did not have a functional CTD during the Georges Bank (1988) study. Large changes in the density field over an hour make this rather inappropriate, in particular for the 10-min averaged data. Since EPSONDE measured the temperature it seemed feasible to estimate the density gradient by using typical temperature–density relationships obtained from CTD observation. We plot the relationship between potential density σ_θ and temperature in Fig. 2 as calculated from CTD temperature and salinity data. We have a relatively good linear correlation between them, and get

$$\sigma_\theta = -0.203T + 27.024, \tag{14}$$

where the correlation coefficient $r = -0.997$. This relationship is used to estimate density and buoyancy frequency for the 10-min averaged EPSONDE temperature data. The noise floor for N^2 is estimated to be 10^{-5} s^{-2} using this relationship. These values of N^2 are then used to calculate K_ρ and R_i in the following sections. The shear estimated from the ADCP and the N^2 estimated from EPSONDE temperature and the relationship between density and temperature from the CTD are matched in vertical scale.

DESCRIPTION OF CTD AND ADCP DATA AT SITE 2B AND SITE 2C

As water flows onto Georges Bank with the tide, colder stratified water from the Gulf of Maine is advected onto the bank (Fig. 1). The time variation of temperature and north–south component of current velocity at Site 213 are shown in Figs 3 and 3b, respectively. We show the on–off bank flow only because it is the dominant one, but in calculating shear the full current is considered. Both temperature and velocity fields are clearly dominated by the semi-diurnal tide. Contoured plots are shown in preference to profiles to illustrate better the temporal progression of the temperature and velocity field. It should be noted that CTD

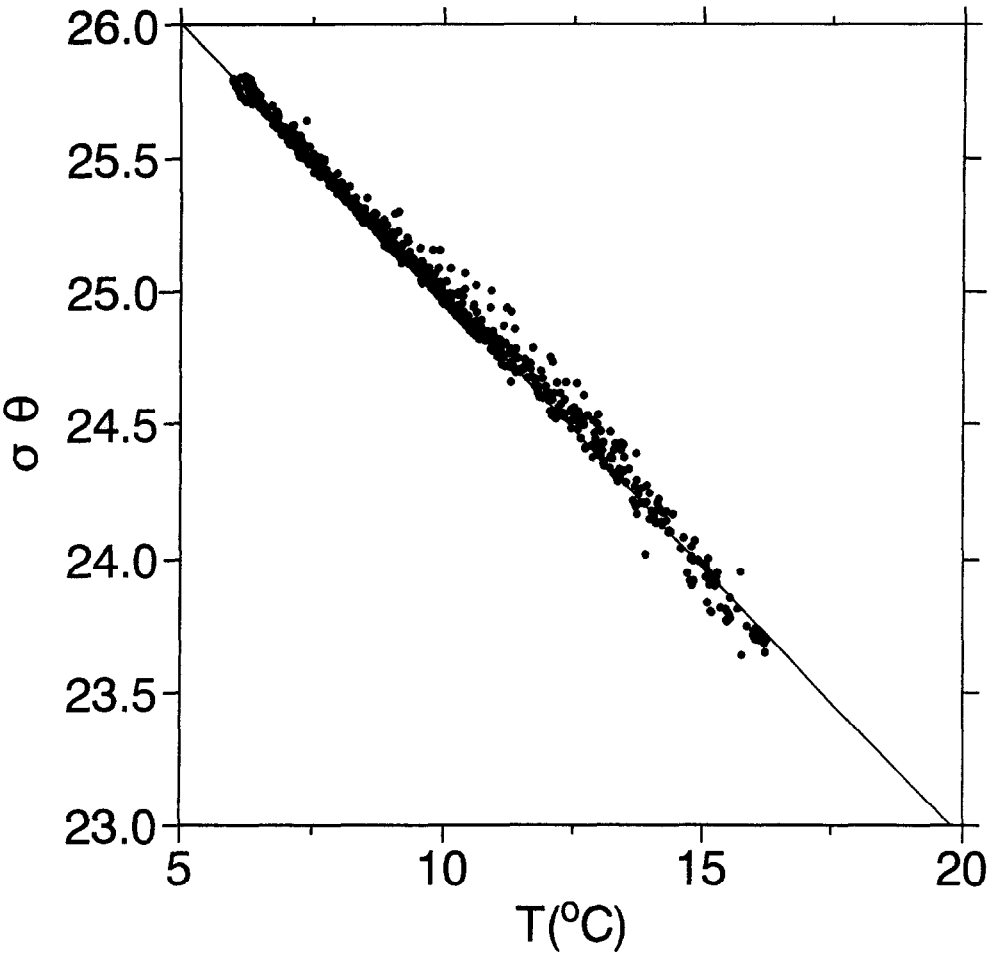

Fig. 2. The temperature–σ_θ relationship for CTD data at Sites 2B and 2C is shown. The linear fit which yields $\sigma_\theta = -0.203T + 27.024$ is shown.

profiles were rarely closer than 5 m from the bottom, so the detailed structure of the bottom boundary layer and its evolution were difficult to deduce. At the start of the figure (Julian day 187.55) the flow is just past maximum on bank, the strongly stratified thermocline exists from about 10 to 20 m depth, and below the thermocline layer, relatively cold homogeneous water less than 6.5°C occupies the site near the bottom. By day 187.65 the current is near ebb and as the current direction changes from southward (on-bank) to northward (off-bank), the front is advected off bank leaving much less stratified water at Site 2, the bottom temperature now approaching 9°C. At the end of northward flow, the stratification is the weakest. The process reverses as the flow turns around and reaches maximum on-bank flow near day 188.05; the deeper water again becomes cold homogeneous water, and the stratification in the shallower layer becomes strengthened. In the thermocline layer at about 15 m depth, internal-wave-like structures appear. Namely, high and low vertical temperature gradient layers alternatively appear at about 15 m depth as time progresses.

A second realization at Site 2, called Site 2C (Fig. 4) starts a few days later on day 193.0. Both temperature and velocity fields are dominated by the semi-diurnal tide in the same manner as at Site 2B. Again as the tide flows off-bank, stratified water is pushed off, then returned as the flow changes on-bank providing maximum stratification near the end of the southward flow. What is remarkable in this section is the occurrence of a very short lived large wave like structure on day 193.13, a large depression of isotherms at the beginning of southward (on-bank) flow. The T–S curve for the anomalous CTD profile is consistent with those for profiles before and after. The signal is strong in conductivity (a reflection of the temperature) and weak in salinity with the density contoured plot (analogous to Fig. 4a, but not shown here) very similar to the temperature contoured plot. This depression suddenly appears on the bank and extends almost the entire depth of the bank, but could not be seen at neighbouring CTD stations an hour before or after, nor was it seen in the temperature records from EPSONDE 20 min before or after. Neither can we see any characteristic features in the velocity field associated with this depression. Although only the cross-bank velocity contours are shown (because they are the strongest signal), neither the along-bank contoured plot or the total rate plot (neither of which are shown here) suggest a velocity structure corresponding to the temperature plot. There is no reason to suspect that these are bogus data: it may be simply a tantalizing occurrence in the CTD record of an internal undular bore. Previous investigations (Loder *et al.*, 1992; Brickman and Loder, 1992) showed that an internal hydraulic jump is sometimes created at the bank edge when the current direction is off-bank, and is accumulated on the bank edge because tidal advection is so large that it prevents the internal wave from propagating on-bank. But, when the tidal current changes its direction southward, the internal wave can propagate on-bank. The observed feature occurs after slack tide as the flow changes from off-bank to on-bank flow. Therefore, this depression may be the passage of such an internal solitary wave. Such features are seen much more readily closer to the bank edge at Site 1. The phase speed of a solitary wave packet (Brickman and Loder, 1992) may be of order $0.35\,\mathrm{m\,s^{-1}}$, which is about half of the flow speed. For a wavelength of $\lambda \approx 300$ m the wave would pass in less than 10 min. Considering the tidal speed and sampling intervals, a feature such as this would be sampled only once with the CTD. In other respects, the stratification on the bank changes as the current direction changes almost as the same manner as that at Site 2B.

EPSONDE DATA AT SITE 2B AND SITE 2C

Hourly averaged data

To compare with the CTD and ADCP observations, the 6–8 EPSONDE microstructure profiles in an hourly BURST were averaged to produce hourly values that were then contoured (Fig. 5). The two basic microstructure measurements of dissipation ε and dissipation of temperature fluctuations χ_T can be understood in the context of the CTD and ADCP data (Fig. 3). ε is highest near the bottom in the two broad time periods, which correspond to maximum off-bank flow at day 187.75 and maximum on-bank flow at 187.95. There are energetic patches ($\varepsilon > 10^{-6}$) well up in the water column when the flow is off-bank. Although the maximum and minimum ADCP velocities are evident in Fig. 3b, the period of maximum flow is also the period of maximum shear in the bottom boundary layer, which is consistent with Fig. 5a. The weakest stratification occurs between off- and on-bank flow. The period of maximum on- or off-bank flow coincides, nevertheless, with weakening

stratification that enhances mixing in the bottom boundary layer. χ_T (Fig. 5b) is less obviously correlated to the mean flow because χ_T depends on both the level of turbulence and the temperature gradient. It is larger for more intense turbulence but smaller if the tetriperature gradient is low. Nevertheless when ε and χ_T are interpreted in the context of vertical diffusivities in Equations (5) and (12) respectively, the contours of K_ρ (Fig. 5c) and K_T (Fig. 5d) again show strong correlations between one another and are highest during periods of strongest flow and highest in the bottom boundary layer.

Highest values of ε, K_ρ and K_T are found near the bottom (below 40 m) when the flow is strongest. At the same time, the lower values found at shallower depths (above the thermocline) also suggest tidal modulation. As the current changes its direction from south to north and gradually increases its speed, high value regions appear near the bottom and develop upward as the current speed is increased. There is no suggestion of a phase lag in development of turbulence, suggesting that at least on time scales of an hour the turbulence is locally generated and dissipated.

In the second times series of turbulence (Fig. 6) at Site 2C, ε, K_ρ and K_T are again highest at the maximum flow (or shear), and in this case it occurs during maximum on-bank flow. Again they are highest near the bottom; K_ρ and K_T are visually correlated. The distribution of χ_T is less strongly correlated to the tide than ε, K_T and K_ρ as at Site 2b. There are, nevertheless, intense patches of χ_T well up in the water column corresponding to the strongest flows. There is little evidence of enhanced mixing associated with the strong temperature anomaly (at day 193.13) shown by the CTD in Fig. 4. In fact there is weaker than normal ε, χ_T, K_ρ and K_T at mid-depth before this, corresponding to minimum tidal velocity as the current goes through a minimum in its switch from off- to on-bank flow. It should be emphasized that no microstructure profiles were made at the same time as the CTD profile where the anomaly was observed. Shortly after the internal wave was observed, high turbulence regions began to develop and progress in the same manner as at Site 2B.

High dissipation layers near the bottom were observed by Dewey *et al.* (1988) near the continental shelf off Vancouver Island. They considered this layer as a turbulent bottom boundary layer, because high dissipation means a high level of turbulent kinetic energy in the layer. Our observations also indicate the existence of a turbulent bottom boundary layer, although for the purpose of the present paper we have not explored it in detail. The EPSONDE microstructure profiler went to the bottom, but the CTD and ADCP did not. Since the focus of the current paper is on the relationship between various indicators of mixing using these three concomitant data sets we simply state that there is an indication of intensive mixing (a bottom boundary layer) strongly correlated with the tide that is stronger near the bottom and reaches well up into the water column.

From Figs 5 and 6 one sees a tendency for microstructure quantities to be relatively higher near the bottom. Nevertheless there are significant levels of turbulence well up in the water column. Integrating ε over the water column at each hourly interval shows (Fig. 7 for Site 2B and Fig. 8 for Site 2C) a good correlation of ε with current, and on average there is at least a five fold increase in integrated ε at times of maximum flow compared to times of minimum flow (Oakey and Pettipas, 1992). Therefore the total turbulent energy changes in response to tidal forcing in the way expected from other studies (such as Dewey and Crawford, 1988). Since it is not the subject of the present paper to explore the bottom boundary layer in detail but rather to explore small time and depth scale correlations of microstructure quantities, we discuss only in passing the relationship between turbulence and mean currents. Preliminary results in Oakey and Pettipas (1992) suggest that integrated dissipation is well

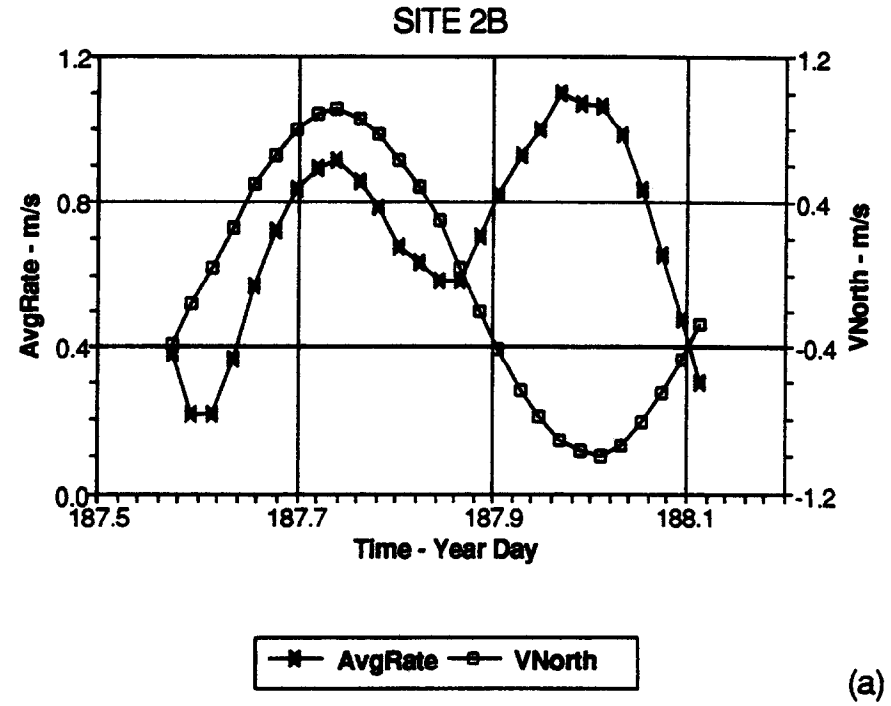
SITE 2B
AvgRate - m/s
VNorth - m/s
Time - Year Day
1.2
0.8
0.4
0.0
-0.4
-1.2
187.5
187.7
187.9
188.1
AvgRate
VNorth

(a)

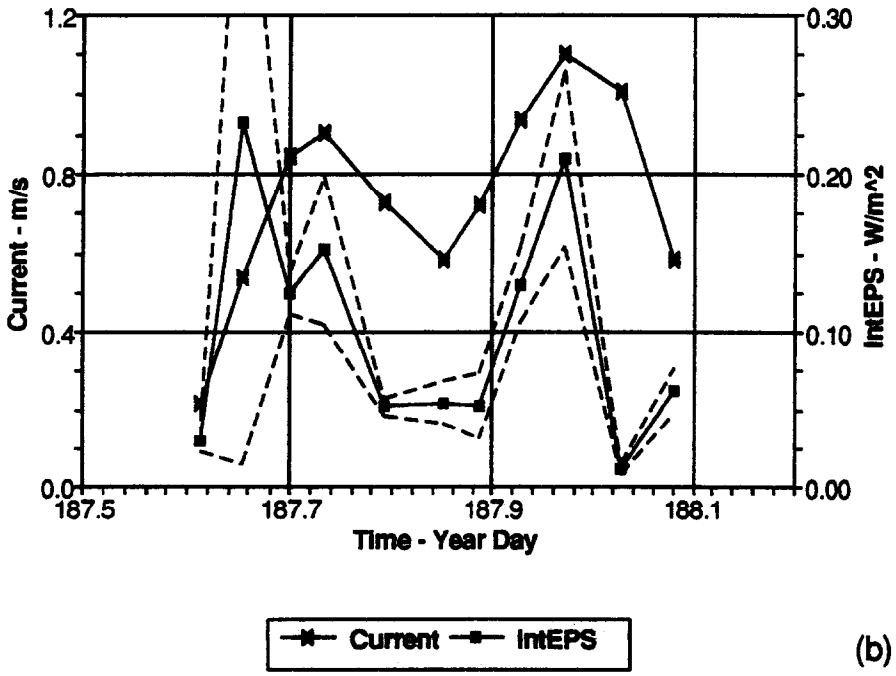
Current - m/s
IntEPS - W/m^2
Time - Year Day
1.2
0.8
0.4
0.0
0.30
0.20
0.10
0.00
187.5
187.7
187.9
188.1
Current
IntEPS

(b)

correlated with U^3, and these results are in preparation separately. While it is evident that depth averaged quantities like ε are be well correlated with the tidal forcing, it will be the challenge of the next sections to explore the characteristics of the mixing.

Ten-minutes averaged data

From the contoured hourly averaged microstructure data it seems apparent that a major component in the parameterization of the turbulent intensity is associated with the tidal velocity or, more realistically, the vertical shear. Regions of high density gradient (high N^2) also represent regions of lower dissipation. Although the forcing is clearly tidal, the time scales associated with turbulent generation and decay suggest that hourly averages are too long a time scale on which to explore the relationships between microstructure quantities. Since the ADCP was recorded at 10 min intervals, the microstructure profiles were averaged into 10 min intervals by combining profiles of dissipation and χ_T to correspond to the mean time of the ADCP data and then contoured. These plots shown in Figs 9 and 10 demonstrate that, as well as reproducing the major features of the hourly contoured data, there are visual correlations to be explored further.

Other than finer temporal resolution and many small scale patches (which results in some blank times and depths indicated as empty boxes) Fig. 9a–9d preserves the essential features of Fig. 5a– 5d for ε, χ_T, K_ρ and K_T, respectively. K_v (Fig. 9e) also shows similar variation to that of K_ρ and K_T. In Fig. 9, N^2 is calculated from EPSONDE temperature and the relation of temperature vs σ_θ [Equation (14)]. Maximum values are in the surface region, a reflection of the higher density gradients, consistent with the temperature contours of Fig. 3a. There is a tendency for ε, K_ρ, K_T and K_v to become large as N^2 becomes small (stratification becomes weak). The velocity shear (Fig. 9h), is rather unexpected, with no clear correlation to the tidal flow and rather uniform through the water column. This is almost certainly a result of the noise associated with the ADCP, suggesting that values of $S^2 < 10^{-5}$ may be affected by instrument noise. This, of course, will affect the calculation of Ri as well, and should give numbers which are too small and rather uniformly distributed. The contoured plot of R_i (Fig. 9f), displays a somewhat complex patterns. Low R_i regions ($R_i < 0.25$) are (surprisingly) distributed over the whole water column and tidal period, but these regions do not necessarily correspond to higher dissipative or higher diffusivities regions. Higher R_i regions, nevertheless, generally correspond to low dissipative or diffusivities regions. For example, after 188.0 Julian day, stratification becomes strong (see Fig. 9g), R_i becomes higher above 35 m depth, and the dissipation and vertical diffusivities decrease.

Similar figures drawn for Site 2C are shown in the same format in Fig. 10. Although the details are different, a consistent pattern to that seen for Site 2B in Fig. 9 is seen. The large temperature anomaly (soliton) is seen in N^2 (Fig. 10g), with a deep high N^2 patch that cuts off mixing as shown by low K_ρ (Fig. 10c) at the time of soliton.

Figures 9 and 10 suggest clear relationships between various microstructure quantities. Although the hourly data also show similar large scale similarities, the time scales for

Fig. 7. The half-hourly depth averaged current at Site 2B along with the half-hourly averaged northward current is shown, (a). Below, (b), is the depth-averaged current interpolated to the time of each hourly averaged burst of microstructure measurements along with the corresponding integrated dissipation from the surface to bottom with standard errors indicated by dashed lines.

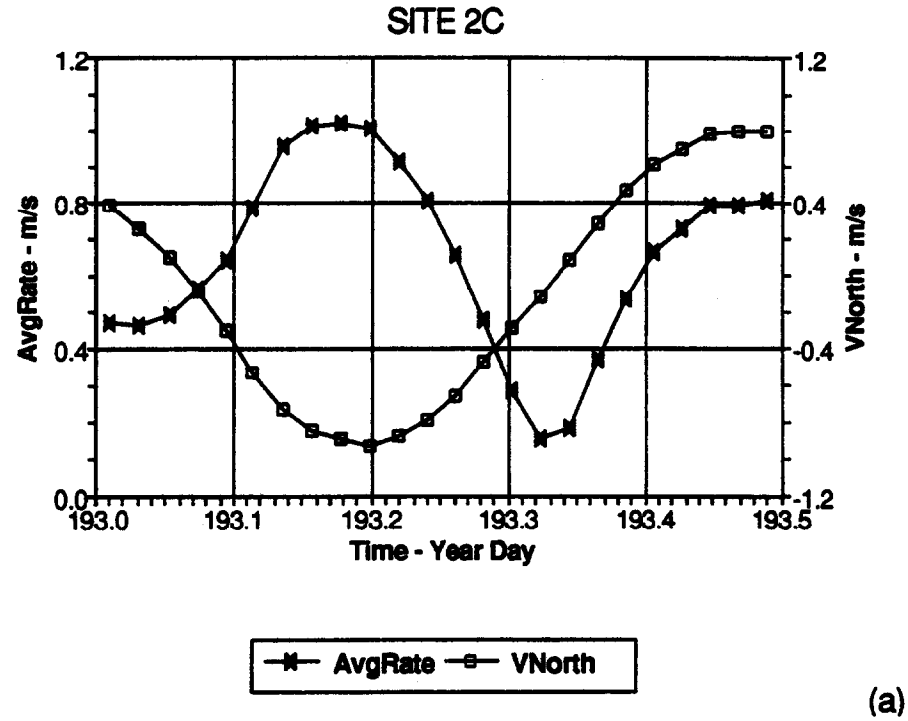
SITE 2C
AvgRate - m/s
VNorth - m/s
Time - Year Day
AvgRate
VNorth

(a)

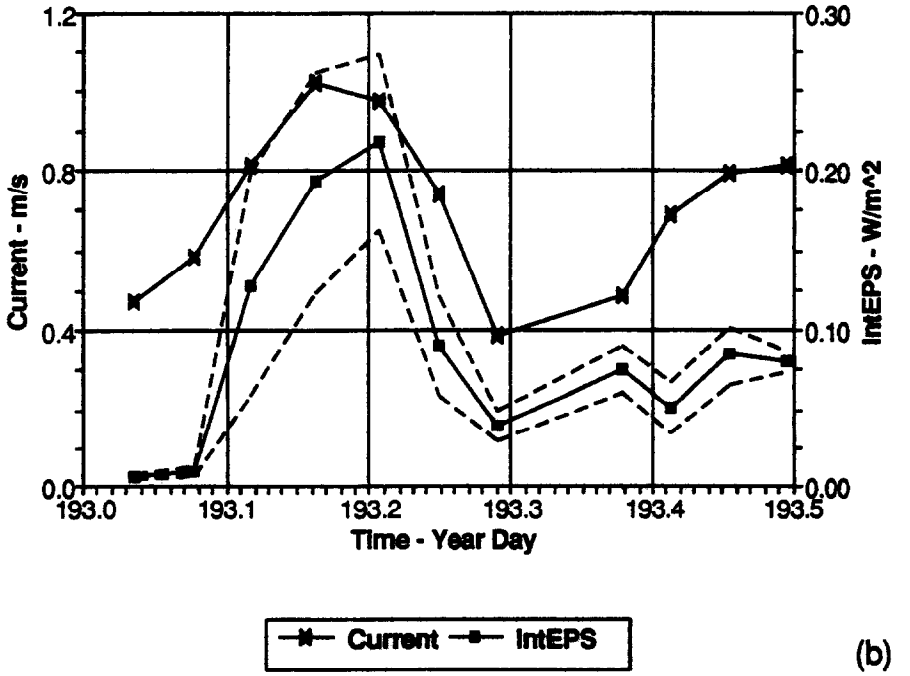
Current - m/s
IntEPS - W/m^2
Time - Year Day
Current
IntEPS

(b)

turbulence generation and dissipation are much shorter than an hour and in fact shorter than the shortest time scale of 10 min available to us. We nevertheless will use the 10-min data to explore different correlations that may exist. This problem of merging data sets on different length and time scales (not unlike the often proposed "nested box" experiments), however, is difficult at best.

STATISTICS OF MICROSTRUCTURE DATA

Matching spatial and temporal scales from a microstructure profiler and an ADCP are compounded by the intermittency of turbulence and the reality that the statistical distributions of turbulent quantities are not normal but strongly skewed. For the discussion to follow, we have grouped all of the data from both Site 2B and Site 2C into one data set for analysis. This data set consists of values of ε, χ_T, K_T, K_ρ and others calculated for each 10-min period and 3.1 m vertical depth interval for which data were available. It also should be noted that each of Site 2B and Site 2C represent a full tidal cycle. The dissipation values at any depth (over a tidal cycle) display a range of at least three orders of magnitude (Fig. 11b). One suitable estimator of the mean at any depth is the arithmetic mean but it is difficult to assign confidence intervals because of the intermittency and skewness of the data. A more appropriate estimator is the maximum likelihood estimator for a log-normal distribution discussed at length by Baker and Gibson (1987). Dissipation rates have been shown to be close to log-normal in surface and benthic mixing layers (Osborn and Lueck, 1985; Shay and Gregg, 1986; Crawford and Dewey, 1990). This would apply to χ_T as well. For other quantities such as K_T and K_ρ our examination of histograms of our data leads us to believe that the log-normal estimator is also appropriate. Briefly, the maximum likelihood estimator (mle) of a log-normal distribution of a random variable X is $\overline{X_{\text{mle}}} = \exp(m + s^2/2)$, where m and s^2 are the arithmetic mean and variance, respectively, of $Y = \ln X$. Confidence intervals including the number of data points, n, in the sample and the degree of confidence, $Z_{\alpha/2}$, (here $Z_{\alpha/2} = 0.98$ corresponding to 68% or one σ confidence level), are then obtained from $\overline{X_{\text{mle}}}\exp(-\eta Z_{\alpha/2}) < \overline{X_{\text{mle}}} < \overline{X_{\text{mle}}}\exp(\eta Z_{\alpha/2})$ where $\eta = [s^2/n + s^4/(2n-1)]^{1/2}$, estimating the variance σ by s. In Fig. 11a this estimator used to calculate the tidally averaged dissipation. For comparison mean $(\ln \varepsilon)$ (o) is also shown to illustrate that it underestimates the dissipation which is dominated by intermittent large values. While this is not an appropriate statistical estimate it is the value often extracted visually as a typical value from a semi-log plot. That $\overline{\varepsilon_{\text{mle}}}$ is also larger that the arithmetic mean in Fig. 11b is a reflection of the large intermittency in the exponent in $\overline{\varepsilon_{\text{mle}}}$. Values of s^2 for these data are of order 4.

Averaged data from the experiment in Fig. 12 show some clear depth dependencies. Dissipation (Fig. 12a) increases with depth by more than an order of magnitude over a tidal cycle with average values of about $2 \times 10^{-6}\,\text{W kg}^{-1}$ near the bottom. χ_T, as noted previously shows little trend with depth, and with a value of order $8 \times 10^{-5}\,\text{C s}^{-2}$. The increase of K_ρ (Fig. 12c) with depth reflects not only the increase of ε with depth but also the decrease of N^2 (Fig. 12g) with depth. K_T (Fig. 12d) generally decreases with depth reflecting the constancy of χ_T with depth and the decrease of N^2 with depth, remembering that N^2 is

Fig. 8. A similar presentation to Fig. 7 is shown for the second time series at Site 2C.

determined largely by the temperature gradient. K_v (Fig. 12e) also decreases with depth reflecting the increase of ε with depth and the decrease of shear, S^2, with depth (Fig. 12h). The Richardson number, R_i, (Fig. 12f) is generally constant with depth, consistent with the decrease of both N^2 and S^2 with depth. Although there are many individual 10-min, 3.1 m bins with $R_i < 0.25$, the mean value over the tidal period is of order 1, still quite small considering the averaging involved. It is clear that the bottom half of the water column is generally very turbulent and actively mixing. The decrease of dissipation in the upper water column is consistent with the observed increased R_i in the upper water column.

Although the general impression of the mixing regime may be inferred from the depth-time averaged data, little can be inferred about the mixing processes. The time and length scales associated with mixing are short compared to this average, and only by examining the statistics of the shorter scales can one explore correctly the interrelationships referred to above. Although the upper water column may be much more complicated as a result of internal waves (and solitons) (Loder *et al.*, 1992), we will explore the statistical relationships between mixing parameters in the data set from the whole water column. Nevertheless, the bottom half of the water column is where we expect the influence of shear and density gradient to be the greatest.

Consider first the dependence on shear, S^2. Microstructure quantities were sorted into 1/3 octave bins of S^2, and the maximum likelihood estimator of the mean and variance (1 σ) were calculated for each bin and are plotted in Fig. 13. Both ε and χ_T appear to increase as the shear increases except at low shear of order 10^{-5} where shear values are suspect because of instrument resolution. Except at low shear values, all of the vertical diffusivities, K_ρ, K_T, and K_v suggest little dependence on shear.

A similar analysis to explore the dependence on N^2 is presented in Fig. 14. From the depth dependence of Fig. 12 one might, for example, assume that because both ε and N^2 showed a depth dependence that ε depends on N^2. This is not the case as is shown in Fig. 14a where ε appears to be nearly independent of N^2. The increase in χ_T at higher N^2 (Fig. 14b) is probably because N^2 is determined mostly by temperature gradient. While K_ρ decreases with increasing N^2 (Fig. 14c) neither K_T or K_v (Figs 14d and e) show any dependence on N^2. The dependence on Richardson number is shown in Fig. 15. As noted earlier, noise in the measurement of shear may result in the calculation of R_i values which are too low. Ignoring the $R_i < 0.1$ data suggests that neither ε or χ_T exhibit a strong dependence on R_i. The diffusivities K_T, and K_v exhibit little dependence on R_i. There is a suggestion that K_ρ may decrease as R_i increases although this is at very low R_i.

$\varepsilon/\upsilon N^2$ is a ratio frequently used in the discussion of stratified turbulence (Gibson, 1980; Stillinger *et al.*, 1983; Gargett, 1988). Often referred to as a turbulent, activity parameter, this ratio may not have universal interpretation depending on the Reynolds number and Froude number associated with the flow (Gargett, 1988). For the flow characteristics of our study site, $\varepsilon/\upsilon N^2$ may be considered to scale as the Reynolds number. The activity parameter except for the constant υ is equivalent to the vertical diffusivity K_ρ. As in the previous comparisons against N^2, S^2 and R_i, the various microstructure parameters have been sorted into bins of $\varepsilon/\upsilon N^2$ (Fig. 16). Not surprisingly, dissipation (Fig. 16a) depends strongly on $\varepsilon/\upsilon N^2$, increasing as the activity parameter increases. χ_T on the other hand (Fig. 16b) increases only slightly with activity parameter. Both measures of the vertical diffusivity K_v and K_T (Fig. 16c and 16d) show a marked increase with this parameter while the ratio of K_v/K_ρ, decreases somewhat (Fig. 16e).

Finally, it is interesting to ask whether the measurements of vertical diffusivity K_ρ and K_T

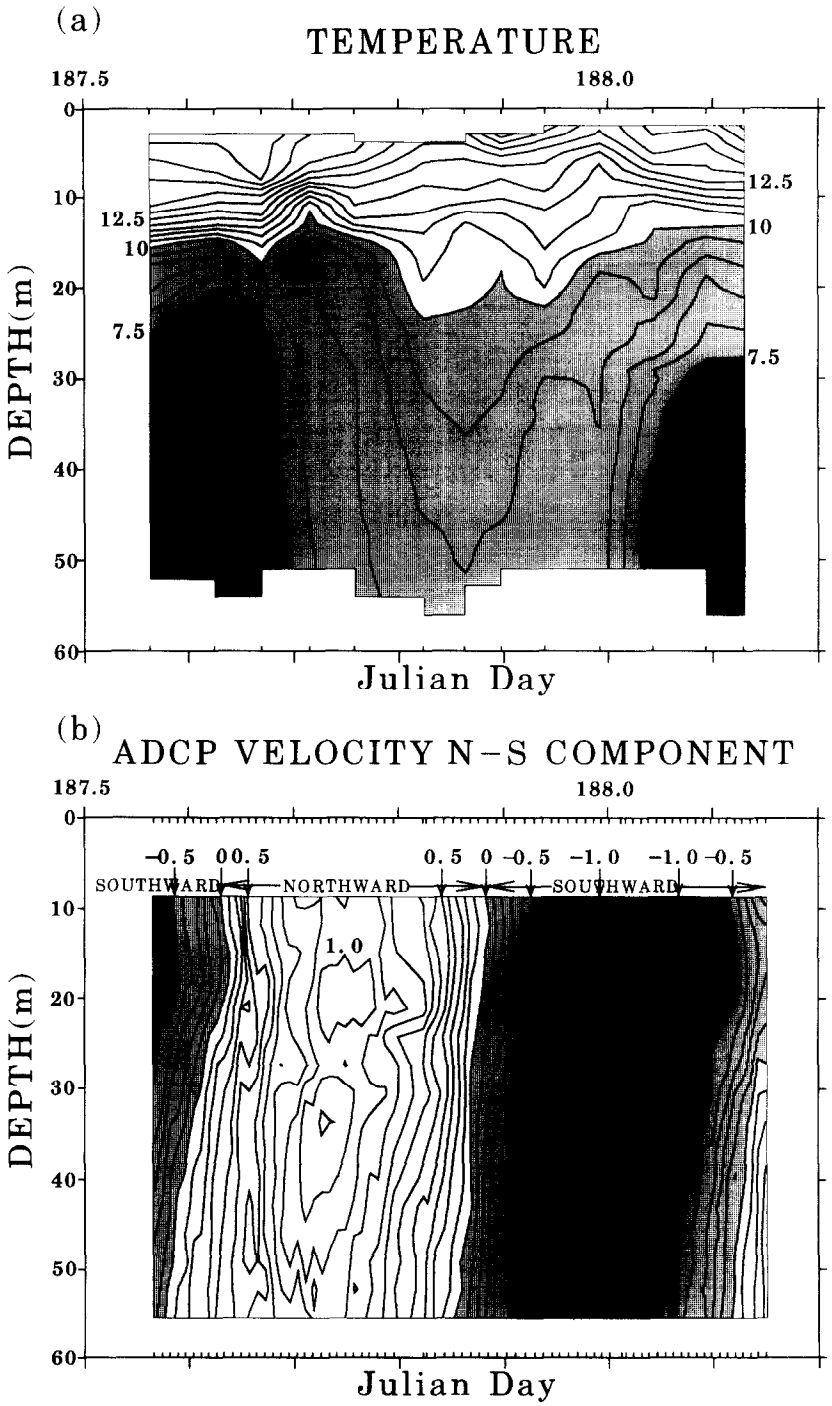

Fig. 3. The time variation of (a) temperature and (b) north–south component of current velocity at Site 2B. The horizontal coordinate is time in Julian Days and the vertical coordinate is depth. Outside tick marks are time marks at an interval of 0.1 day. Inside tick marks show the time when CTD and ADCP data were obtained. Contour lines were plotted by using NCARG (National Center for Atmospheric Research Graphic) package. Linear interpolation is used in this package. Contour intervals are 0.5°C for (a) and 0.1 m s^{-1} for (b).

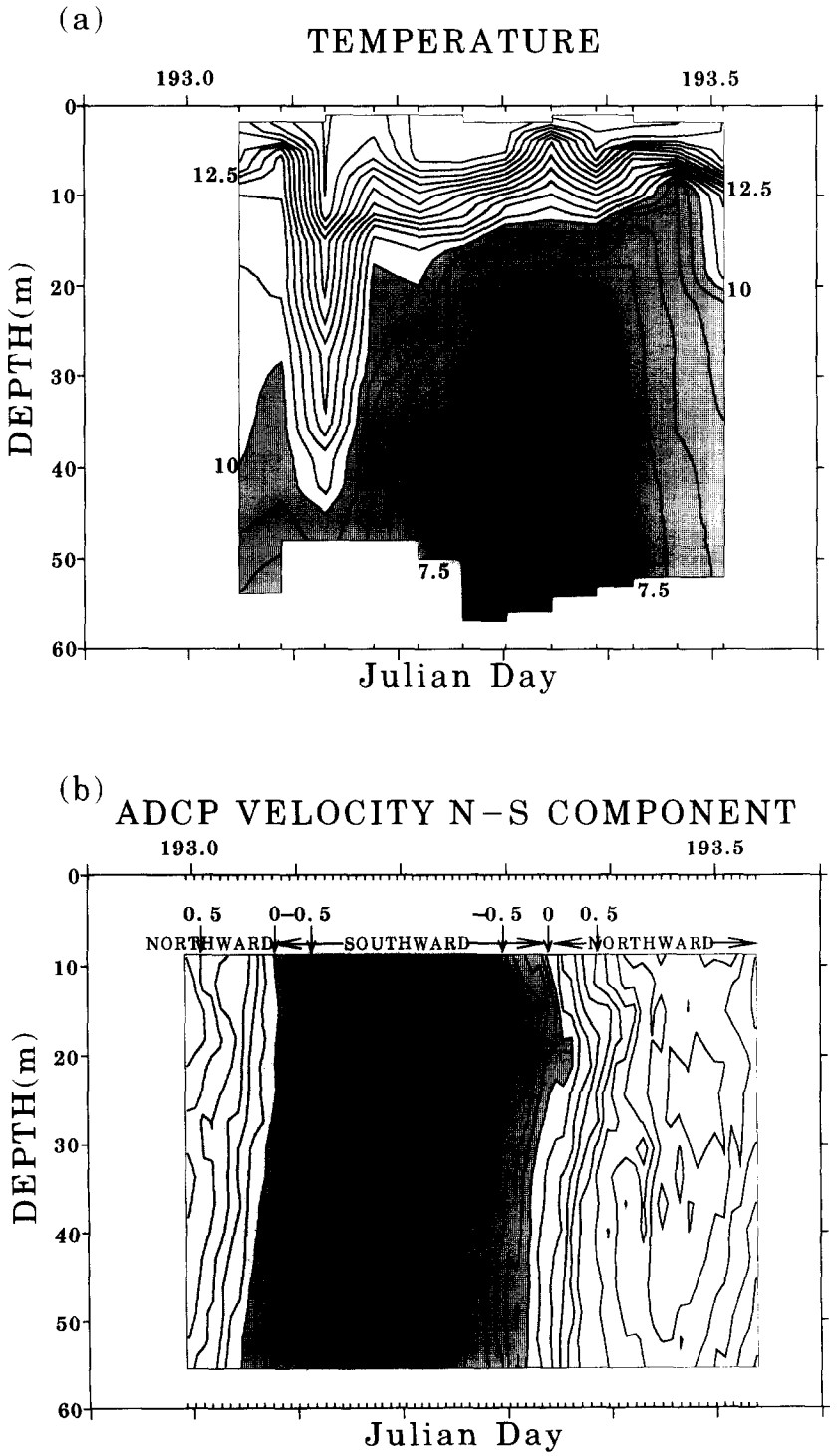

Fig. 4. The same as in Fig. 3, but at Site 2C. Of special interest is the strong internal wave or soliton at day 193.13.

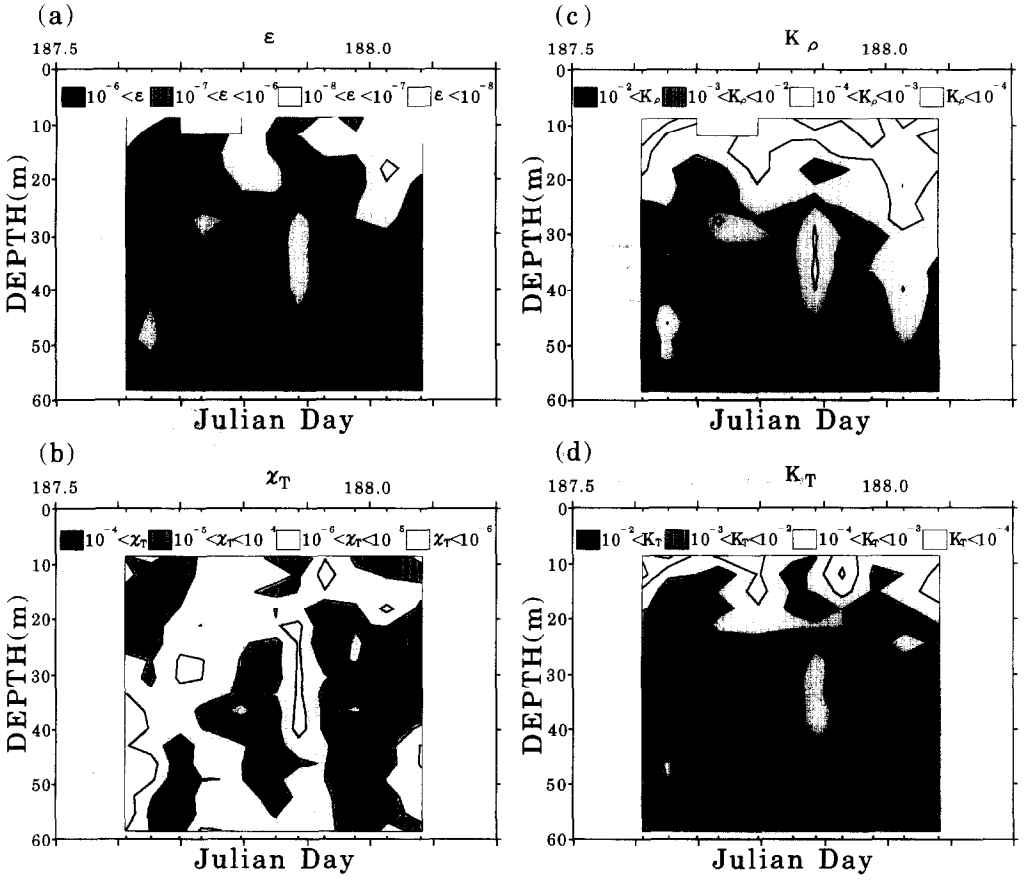

Fig. 5. The time variation of hourly averaged (a) ε, (b) χ_T, (c) K_ρ and (d) K_T at Site 2B. The horizontal coordinate is the time in Julian Days and the vertical coordinate is depth. Outside tick marks are time marks at an interval of 0.1 day. Inside tick marks show the time when EPSONDE data were averaged. The contour interval is -1.0 in logarithmic scale.

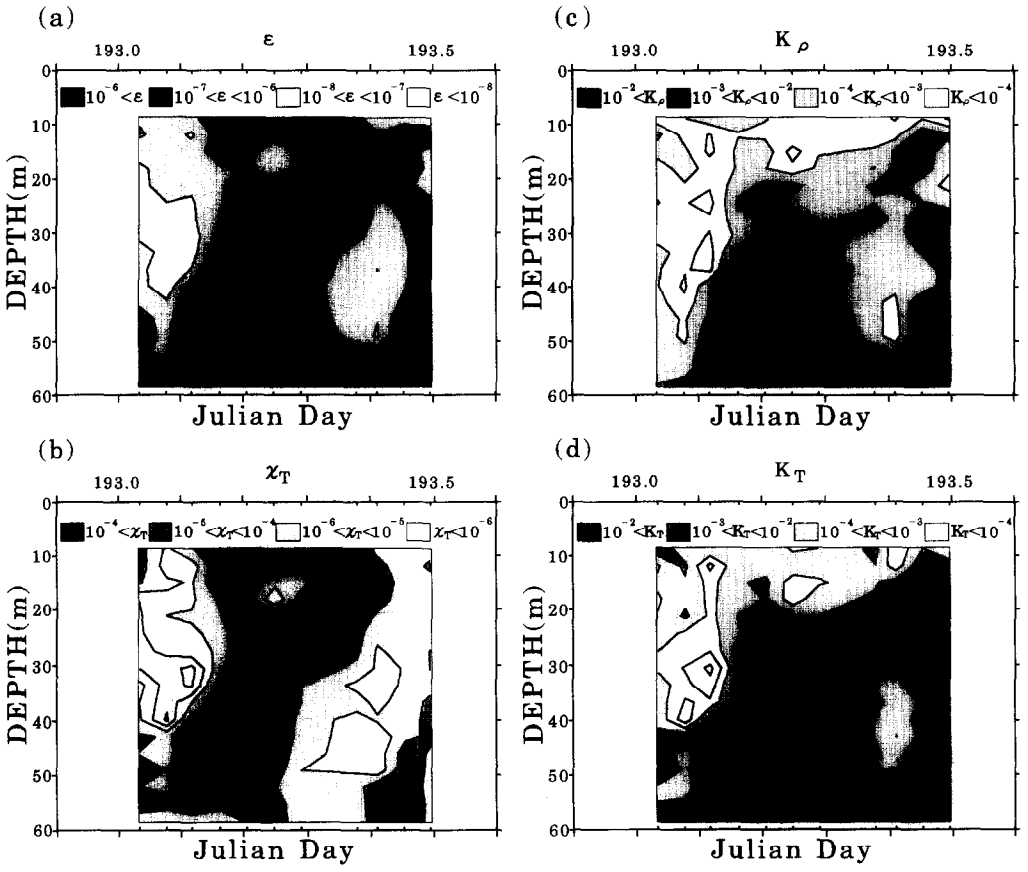

Fig. 6. The same as in Fig. 5, but at Site 2C.

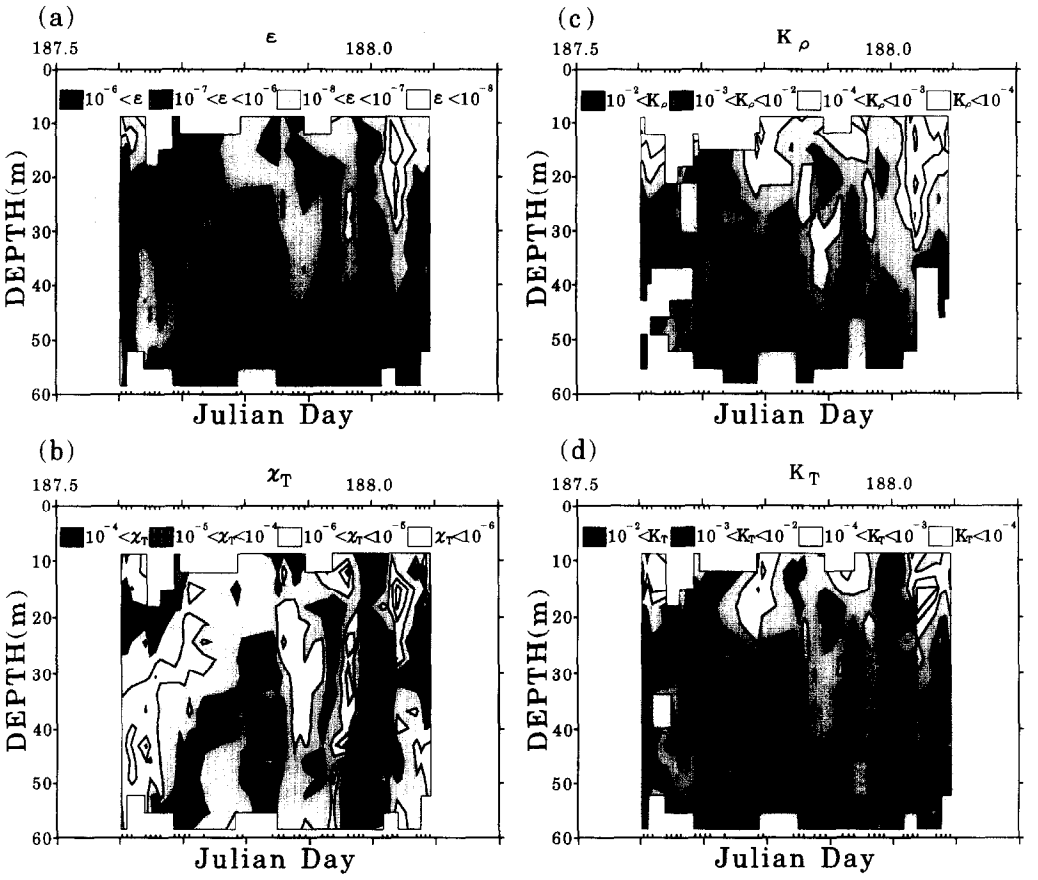

Fig. 9. The time variation of 10 min averaged (a) ε, (b) χ_T, (c) K_ρ, (d) K_T, (e) K_ν, (f) R_i, (g) N^2 and (h) S^2 at Site 2B. Blanks in these figures are due to the lack of data. In other respects the figure is the same as Fig. 5. Note that R_i is contoured at 0.25, 0.5, 1.0, 10.0. (*Continued overleaf.*)

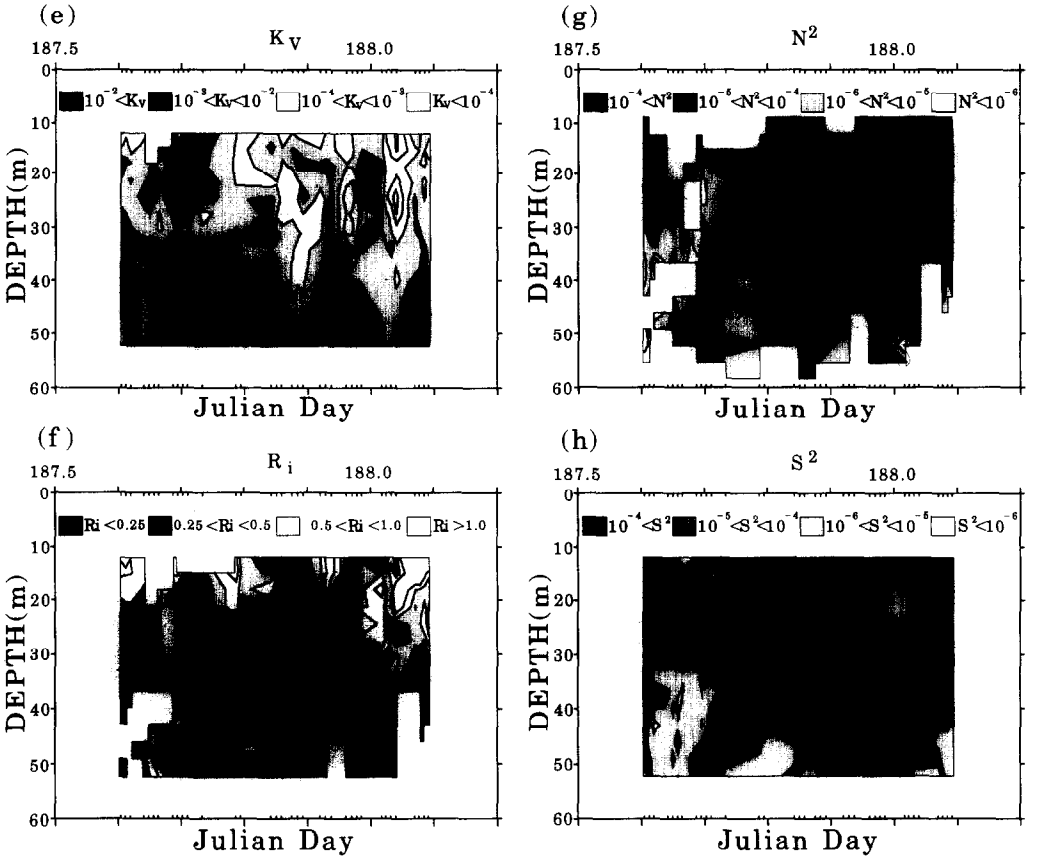

Fig. 9. (*Continued.*)

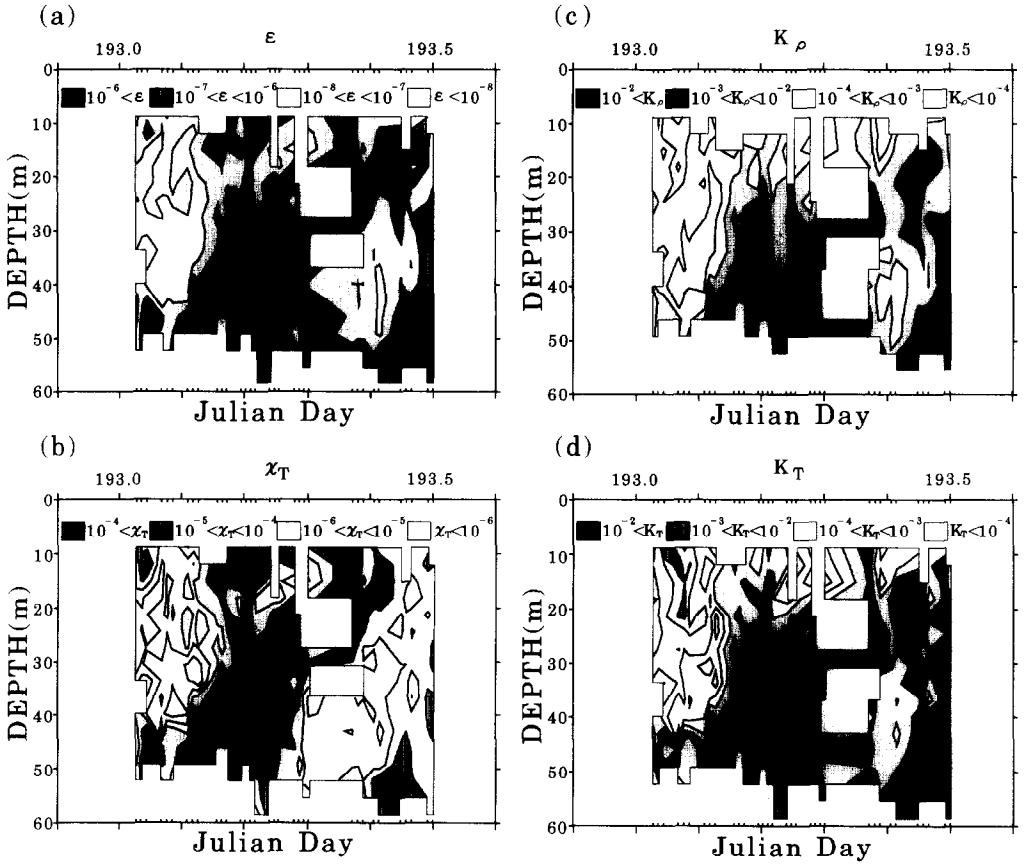

Fig. 10. The same as in Fig. 9, but at Site 2C.

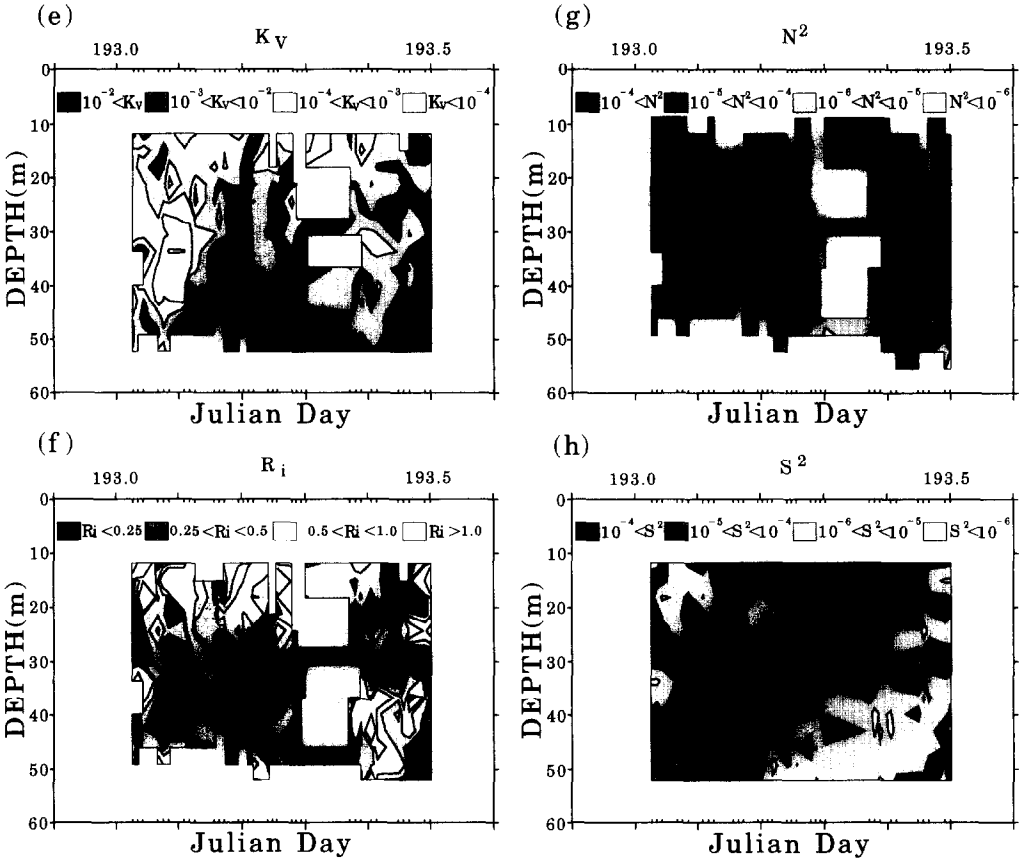

Fig. 10. (*Continued.*)

yield similar estimates of mixing. This is done by looking at the distribution of the ratio of K_T to K_ρ versus S^2, N^2, R_i and $\varepsilon/\upsilon N^2$. A scatter plot of this ratio against S^2 (Fig. 13f) shows little evidence of any dependence. A similar plot of the ratio against N^2 (Fig. 14f) suggests a positive correlation. The ratio appears to decrease at $R_i < 0.1$ (Fig. 15f) although the scatter makes any dependence speculative. K_T/K_ρ shows little dependence on $\varepsilon/\upsilon N^2$.

DISCUSSION AND SUMMARY

From the data presented in the previous sections, the tidal mixing front at the northern flank of Georges Bank is a complex turbulent regime. It is strongly forced, particularly in the bottom boundary layer, yielding high levels of turbulent energy dissipation. Values of $\varepsilon > 10^{-6}$ averaged over a tidal cycle are three orders of magnitude larger than found in the main pycnocline of the ocean (Gregg and Sanford, 1988; Burke, 1994) and significantly larger than values found in regions such as the equatorial undercurrent (Peters *et al.*, 1988; Hebert *et al.*, 1991). The dissipation increases strongly towards the bottom and the integrated dissipation is well correlated to the mean current. The depth dependence observed agrees in general with the Horne *et al.* (1995) results although they observe more energy near the surface, presumably as a result of surface forcing. Horne *et al.* show more turbulent energy dissipation at the mixed site and somewhat less at the frontal site than we observe at Site 2B and 2C. We believe the results to be consistent, however, reflecting a different stratification between the two times of the season for the two studies and the fact that the tidal strength is somewhat higher in our study than in theirs.

Some attempt was made to explore the way various microstructure and turbulence measurables on Georges Bank may be related to other, generally larger scale quantities that are more usually thought to be related to the generation of turbulence. The 10-min averaged data set that was used can only be described as "noisy" because of the difficulty of matching in time and space the measurements from three different instruments. It might seem to be more appropriate to use data averaged over longer times, for example hourly averaged data. This was rejected because the temporal and spatial scales associated with turbulence generation and dissipation are much shorter than this. Turbulent time scales $(\upsilon/\varepsilon)^{1/2}$ are much less than a minute and the time scales associated with the largest eddies of order N^{-1}. Although on scales of an hour the tidal forcing changes significantly, on the time scales of the microstructure and dissipation measurements the processes are assumed to be locally in balance.

The 10-min data set includes parameter values from within 5–8 m of the bottom to within at least 10 m from the surface. Unfortunately this does not include much of the bottom boundary layer, which contains the regions of strongest shear and smallest density gradients. It is perhaps for this reason that dependence of ε on shear is shown to be weak (Fig. 13a). Considering the intense mixing events at the bottom at maximum tidal flow (Figs 5 and 6) the dependence on shear may be stronger. Mean dissipation shows no significant dependence on N^2 or R_i, although the standard errors are large. The dependence of ε on N^2 has been discussed widely in relation to a number of oceanographic situations. For internal wave field dynamics, McComas and Muller (1981) predicted $\varepsilon \propto N^2$ based on the weak-wave interaction theory. Gregg and Sanford (1988) tested this relation in the California coastal region. On the other hand, other observations suggested that $\varepsilon \propto N$. Gargett (1989) discussed the importance of this dependence in mixing processes in the interior of the ocean. For shear-generated turbulence generated by the internal wave field ε is expected to be

dependent on N to a power between 1 and 2. Internal waves might be important in the generation of mixing higher in the water column, but certainly they are unlikely to be important near the bottom where tidally generated shear is more appropriate. For the present study there is no evident ε dependence on N, but there is a strong dependence of dissipation on $\varepsilon/\upsilon N^2$ (Fig. 16a). Since we showed that there was little of ε dependence on N^2 (Fig. 14a), the dependence may be little more than a plot of ε versus ε.

Of greater interest than the dissipation are perhaps the vertical diffusivities. The magnitude is important to other processes on the Bank such as nutrient regeneration and biological productivity. As well we are interested in the inter-relationship of K_T, K_v and K_ρ to one another and to forcing related quantities such as S^2, N^2, R_i and $\varepsilon/\upsilon N^2$. In the relation between K_ρ and K_T, if the density stratification is mainly determined by temperature then by the definitions of equations (3) and (10) one would expect them to be equal, or at least proportional if the "mixing efficiency" Γ is a constant. We have used the value of $\Gamma = 0.25$ (Oakey, 1985), but other investigations have shown different values (Peters *et al.*, 1988; Yamazaki and Osborn, 1990). Although values of Γ found in different experiments range down to about 0.05, theory would suggest that $\Gamma = 0.25$ should be an upper limit (Osborn, 1980). For $K_T = K_\rho$ the correct Γ is given by $\Gamma_c = \Gamma \times K_T/K_\rho$ (Oakey, 1988a). We have calculated the ratio K_T/K_ρ and plotted it against S^2, N^2, R_i and $\varepsilon/\upsilon N^2$ to examine whether the mixing efficiency depends on any of these parameters. There is no clear dependence on shear; the arithmetic mean of the distribution is approximately unity although the scatter is several orders of magnitude. There is a clear tendency for Γ to be smaller at smaller N^2 or lower stratification. There is no strong relationship between Γ and $\varepsilon/\upsilon N^2$ (Fig. 16f).

From the definition of K_ρ and K_v [equations (5) and (7)] we have a relationship $K_v = \frac{R_i}{\Gamma} K_\rho$. Previous measurements (Peters *et al.*, 1988) suggest a dependence $K_\rho \propto R_i^{-n}$. Our results suggest no dependence of K_v on R_i or $n = 1$ which means that $K_\rho \propto R_i^{-1}$ up to $R_i = 1$ (Fig. 15c).

From the CID, ADCP and EPSONDE microstructure observations, on Georges Bank, several interesting features on the mixing processes were found.

1. Highest dissipation and diffusivity regions appear near the bottom of the Bank. High dissipation rate in the layer means a high level of turbulent kinetic energy, which contributes to higher mixing rates. Values of dissipation averaged over a tidal cycle were found to be well in excess of 10^{-6} W kg^{-1} in the lower 20 m of the water column.

2. The turbulent region near the bottom changes its thickness as tidal flow on the bank changes its phase. Intense mixing extends as high as 30–40 m when the on-bank (southward) flow is strongest, and stratification is weak. Although a detailed study of the dependence of bottom boundary layer thicknesses related to the strength of the tidal forcing has not been done, our results are visually similar to those observed by Dewey *et al.* (1988) near Vancouver Island where strong tidal flow also dominates the behavior of the turbulent bottom boundary layer.

3. The intensity of dissipation and χ_T curiously showed only a small dependence on S^2, which may reflect simply the difficulty of matching ADCP data to microstructure data.

Fig. 11. The dissipation data from Site 2B and Site 2C is displayed as 10 min averages at all depths and times corresponding to ADCP measurements in panel (b) with the arithmetic mean of the data shown as a solid line. In panel (a) the average profile is shown as the median [circles, obtained from mean (ln ε)] and as the log-normal maximum likelihood estimator (+) with standard errors.

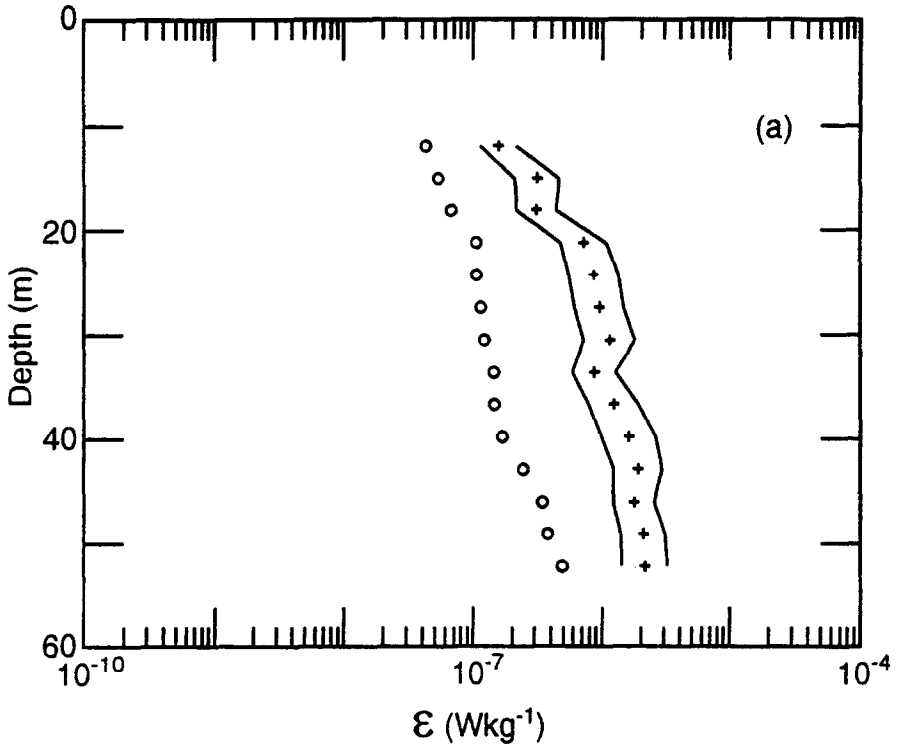
0
20
40
60
Depth (m)
(a)
10^{-10}
10^{-7}
10^{-4}
ε (Wkg^{-1})

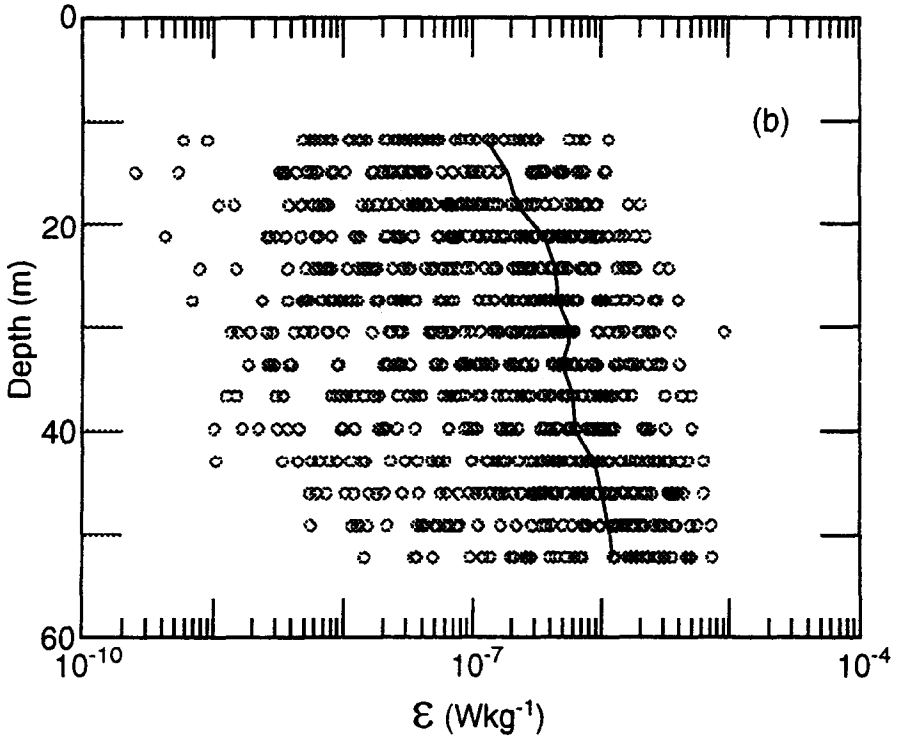
0
20
40
60
Depth (m)
(b)
10^{-10}
10^{-7}
10^{-4}
ε (Wkg^{-1})

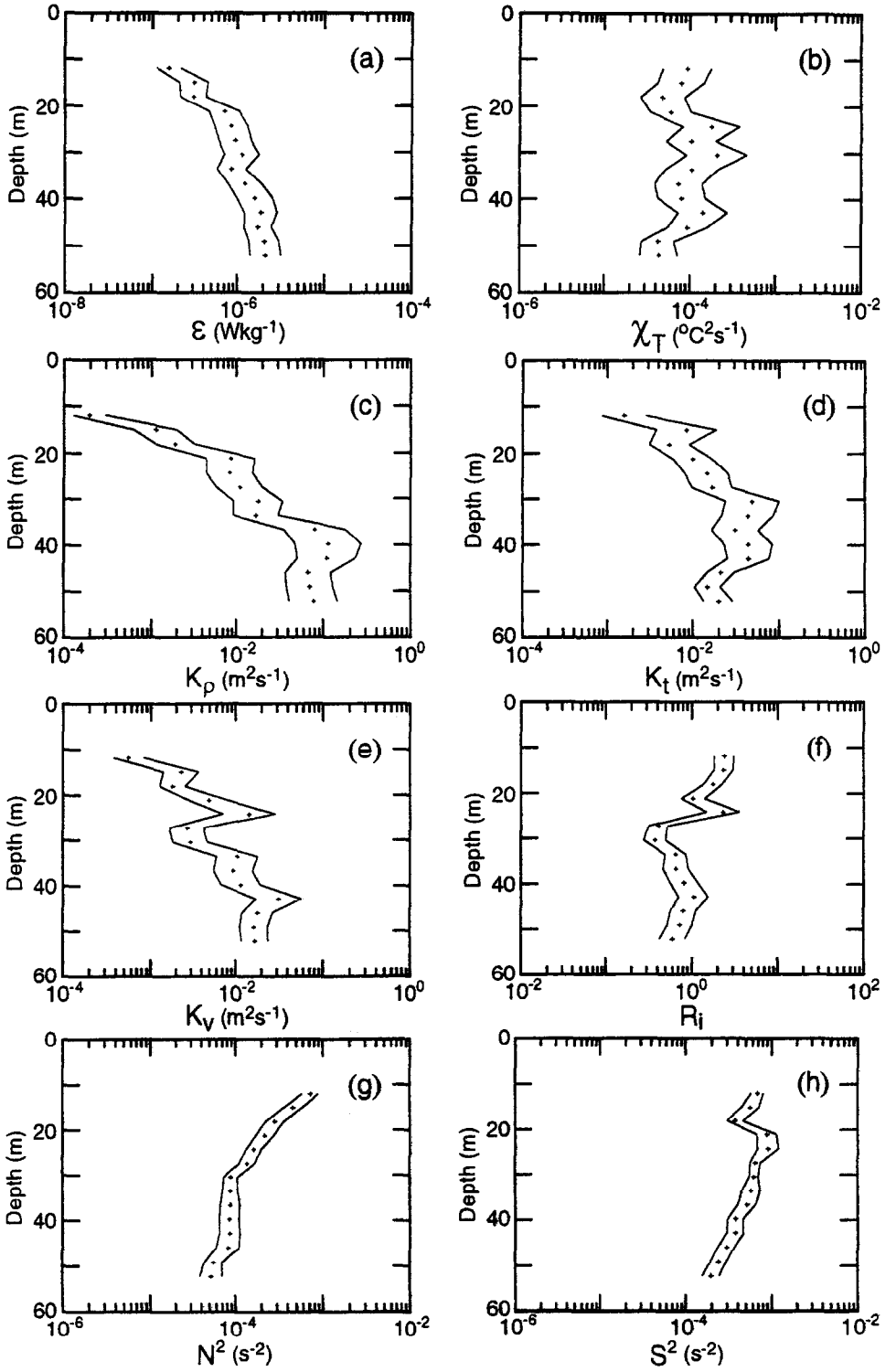
(a)
Depth (m)
0
20
40
60
10^{-8}
10^{-6}
10^{-4}
ε (Wkg^{-1})
(b)
10^{-6}
10^{-4}
10^{-2}
χ_T (°C^{2}s^{-1})
(c)
10^{-4}
10^{-2}
10^{0}
K_ρ (m^{2}s^{-1})
(d)
K_t (m^{2}s^{-1})
(e)
K_v (m^{2}s^{-1})
(f)
10^{2}
R_i
(g)
N^2 (s^{-2})
(h)
S^2 (s^{-2})

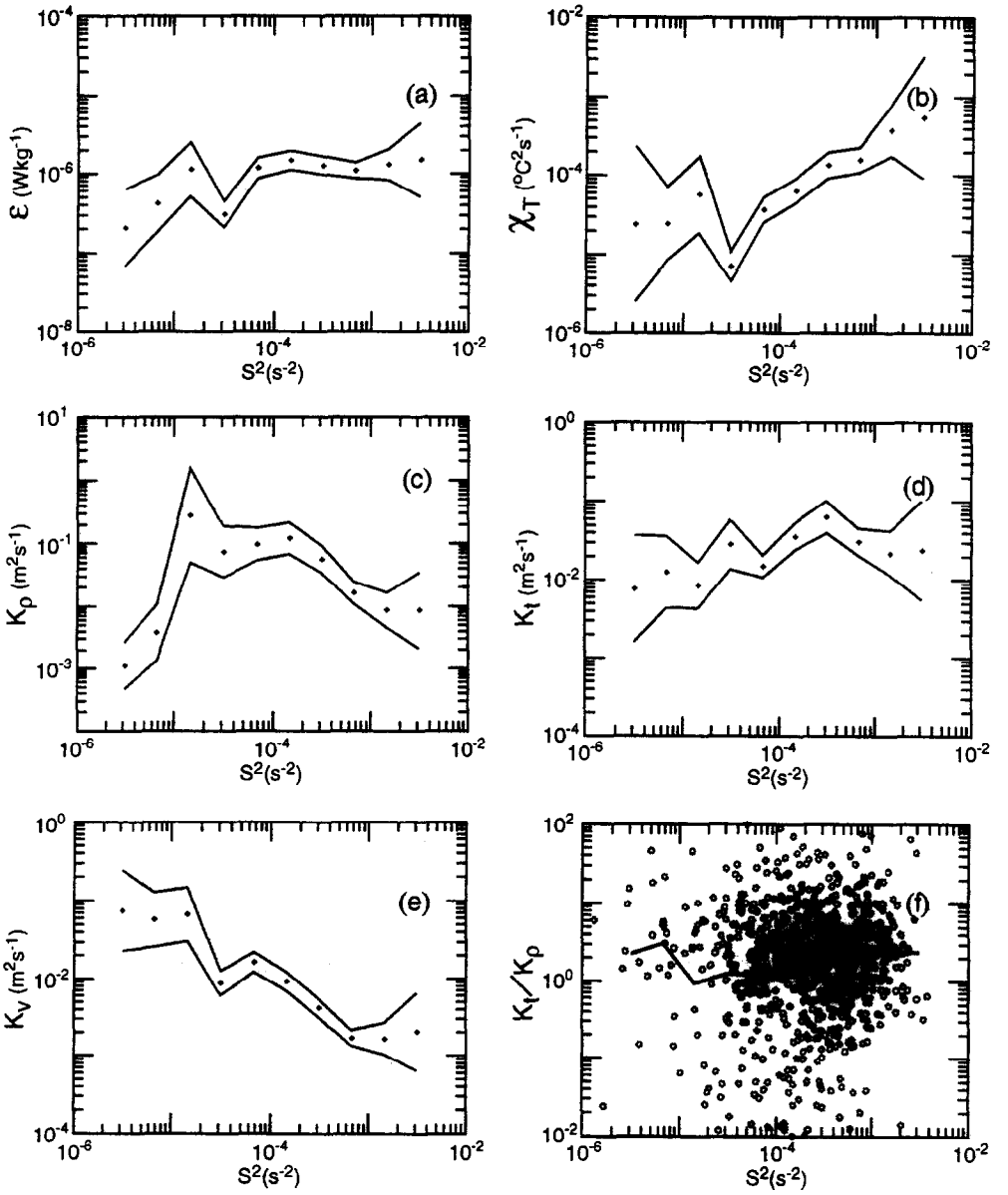

Fig. 13. The relationship of (a) ε, (b) χ_T, (c) K_ρ, (d) K_T, (e) K_v, (f) K_T/K_ρ to S^2 binned in 1/3 octave bands is shown for the data from Site 2B and Site 2C.

Fig. 12. Depth-averaged mean profiles are shown corresponding to the panels of Figs 9 and 10. In each panel the vertical axis is depth and the horizontal axis is the microstructure or calculated quantity. In each case the profile (+) is the maximum likelihood estimator of the quantity and the solid lines define the one σ confidence intervals. The profiles summarize all of the data from Sites 2B and 2C.

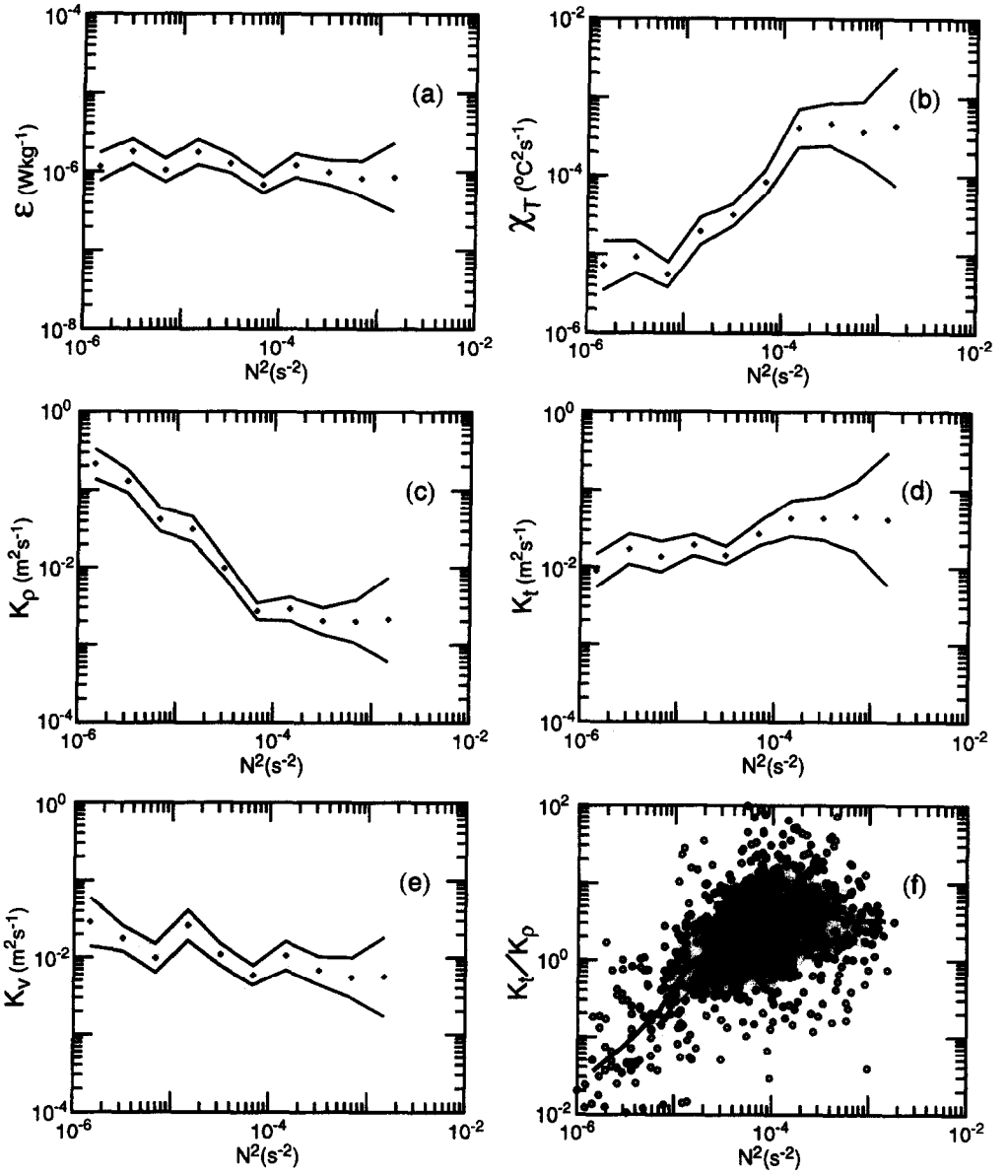

Fig. 14. The relationship of (a) ε, (b) χ_T, (c) K_ρ, (d) K_T, (e) K_ν, (f) K_T/K_ρ to N^2 binned in 1/3 octave bands is shown for the data from Site 2B and Site 2C.

Dissipation appeared to be independent of N^2 and decreased somewhat at higher R_i. χ_T increased at higher N^2, indicating that as the density (temperature) gradient increased there was more mixing. This is also evident in a small increase in χ_T as $\varepsilon/\upsilon N^2$ increases.

4. The vertical diffusivities K_T, K_ρ and K_ν all are highest near the bottom and are in excess of $10^{-2}\,\mathrm{m^2\,s^{-1}}$. The mixing efficiency (represented by the ratio K_T/K_ρ) shows little dependence on S^2, R_i of $\varepsilon/\upsilon N^2$. There is evidence suggesting that the mixing efficiency decreases with increasing N^2.

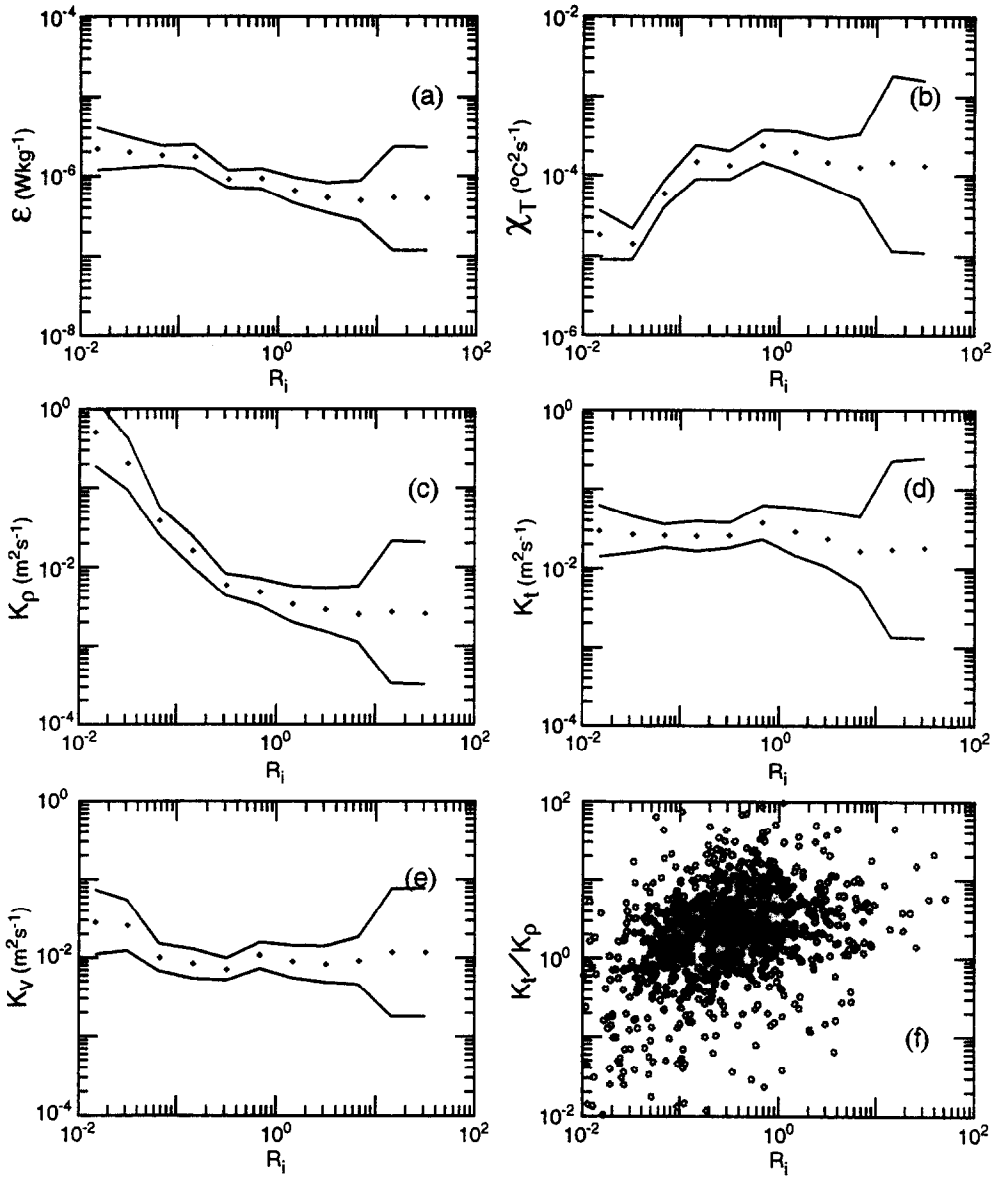

Fig. 15. The relationship of (a) ε, (b) χ_T, (c) K_ρ, (d) K_T, (e) K_v, (f) K_T/K_ρ to R_i binned in 1/3 octave bands is shown for the data from Site 2B and Site 2C.

Acknowledgements—Jiro Yoshida was funded by the Fund for Research Encouragement in Celebration of the Centennial Anniversary of the Founding of Tokyo University of Fisheries. This fund enabled him to stay at Bedford Institute of Oceanography in 1991. He also expresses his thanks to Allyn Clarke for his hospitality to permit J.Y. to stay at BIO. We express our thanks to John Loder, Ed Horne, Ken Drinkwater and Dave Brickman for their discussions. Thanks are also extended to Hidekatsu Yamazaki, Hideki Nagashima and Masaji Matsuyama for their advice. Neil Oakey would like to acknowledge his collaborators in the Georges Bank (1988) study, Ed Horne and in particular John Loder, whose scientific leadership in the study was crucial. The field staff and data processing staff deserve a thank-you for their help.

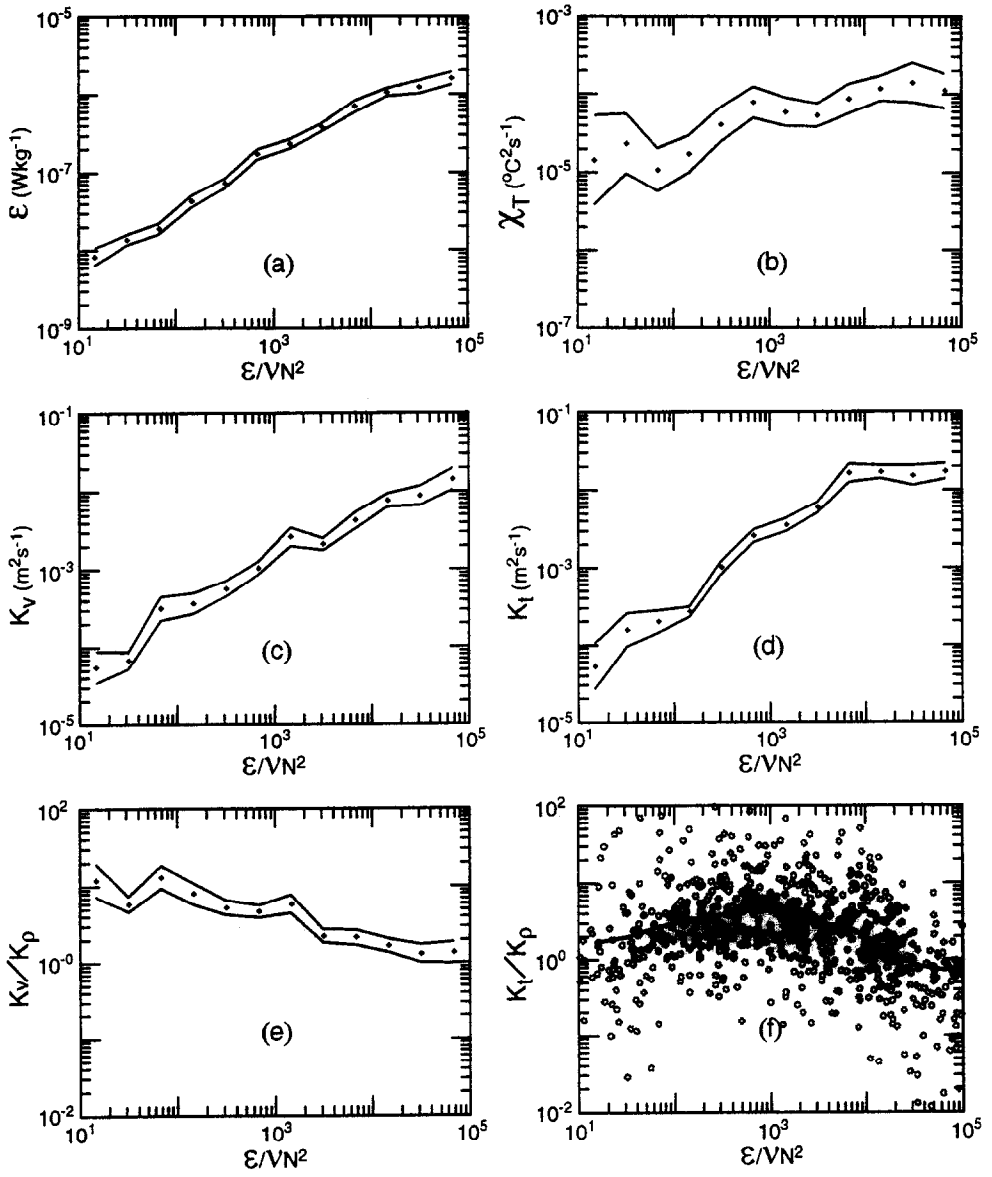

Fig. 16. The relationship of (a) ε, (b) χ_T, (c) K_v, (d) K_T, (e) K_v/K_ρ and (f) K_t/K_ρ to $\varepsilon/\upsilon N^2$ binned in 1/3 octave bands is shown for the data from Site 2B and Site 2C.

REFERENCES

Baker M. A. and C. H. Gibson (1987) Sampling turbulence in the stratified ocean: statistical consequences of strong intermittency. *Journal of Physical Oceanography*, **17**, 1817–1836.

Brickman D. and J. W. Loder (1992) The energetics of the internal tide on northern Georges Bank. *Journal of Physical Oceanography*, **23**, 409–424.

Burke J. F. (1994) Analysis of microstructure data from the North Atlantic Tracer Release Experiment, M.Sc. Thesis, Dalhousie University, 112 pp.

Cochrane N. A. (1985) An operational evaluation of an Ametek Straza, DCP-4400 300 kHz doppler current profiler aboard the CSS Dawson, Canadian Technical Report, Hydrographic Ocean Science, no. 68, 52 pp.

Crawford W. R. and R. K. Dewey (1990) Confidence limits for friction velocities determined from turbulence profiles in coastal waters. *Journal of Atmospheric and Oceanic Technology*, **7**, 50–57.

Dewey R. K. and W. R. Crawford (1988) Bottom stress estimates from the vertical dissipation rate profiles on the continental shelf. *Journal of Physical Oceanography*, **18**, 1167–1177.

Dewey R. K., P. H. LeBlond and W. R. Crawford (1988) The turbulent bottom boundary layer and its influence on local dynamics over the continental shelf. *Dynamics of the Atmosphere and Oceans*, **12**, 143–172.

Gargett A. (1988) The scaling of turbulence in the presence of stable stratification, *Journal of Geophysical Research*, **93**, 5021–5036.

Gargett A. E. (1989) Ocean turbulence. *Annual Reviews in Fluid Mechanics*, **21**, 419–451.

Gibson C. H. (1980) Fossil temperature, salinity and velocity turbulence in the ocean. In: *Marine turbulence*, C. J. Nihoul, editor, Elsevier Science, New York, pp. 221–258.

Gregg M. C. and T. B. Sanford (1988) The dependence of turbulent dissipation on stratification in a diffusively stable thermocline. *Journal of Geophysical Research*, **93C10**, 12381–12392.

Hebert D., J. N. Mouni and D. R. Caldwell (1991) Does ocean turbulence peak at the Equator?: revisited. *Journal of Physical Oceanography*, **21**, 1690–1698.

Hinze J. O. (1975) *Turbulence*, 2nd edn, McGraw-Hill series in Mechanical Engineering, NY, 618 pp.

Horne E. P. W., J. W. Loder, W. G. Harrison, R. Mohn, M. R. Lewis, B. Irwin and T. Platt (1989) Nitrate supply and demand at the Georges Bank tidal front. *Topics in Marine Biology, Scient. Mar.*, **53**, 145–158.

Horne E. P. W., J. W. Loder, C. E. Naimie, and N. S. Oakey (1995) Turbulence dissipation rates and nitrate supply in the upper water column on Georges Bank. *Deep-Sea Research II*, **43**, 1683–1712.

Loder J. W. and T. Platt (1985) Physical controls on phytoplankton production at tidal fronts. In: *Proceedings of the 19th European Marine Biology Symposium*, P. E. Gibbs, editor, Cambridge University Press, Cambridge, U.K., pp. 3–21.

Loder J. W., R. G. Pettipas, D. J. Belliveau (1990) Itercomparison of current measurements from the Georges Bank frontal study. Canadian Technical Report, Hydrographic Ocean Science, no. 127, 75 pp.

Loder J. W., D. Brickman and E. P. W. Horne (1992) Detailed structure of currents and hydrography on the northern of Georges Bank, *Journal of Geophysical Research*, **97**, 14,331–14,351.

Loder J. W., K. F. Drinkwater, N. S. Oakey and E. P. W. Horne (1993) Circulation, hydrographic structure and mixing at tidal fronts: The view from Georges Bank. *Philosophical Transactions of the Royal Society of London, Series A*, **343**, 447–460.

McComas C. H. and P. Muller (1981) The dynamic balance of internal waves. *Journal of Physical Oceanography*, 970–986.

Oakey N. S. (1985) Statistics of mixing parameters in the upper ocean during JASIN phase 2. *Journal of Physical Occanography*, **15**, 1662–1675.

Oakey N. S. (1988a) Estimates of mixing inferred from temperature and velocity microstructure. In: *Small scale turbulence and mixing in the ocean*, C. J. Nihoul and B. M. Jamart, editors, Elsevier, Oxford, pp. 239–248.

Oakey N. S. (1988b) EPSONDE: an instrument to measure turbulence in the deep ocean. *IEEE Journal of Oceanic Engineering*, **13**, 124–128.

Oakey N. S. and R. G. Pettipas (1992) Vertical mixing rates on Georges Bank during June–July and October, 1988, Canadian Technical Report, Hydrographic Ocean Science, no. 110, 226 pp.

Osborn T. R. (1980) Estimates of the local rate of vertical diffusion from dissipation measurements. *Journal of Physical Oceanography*, **10**, 83–89.

Osborn T. R. and C. S. Cox (1972) Oceanic fine structure. *Geophysical Fluid Dynamics*, **3**, 321–345.

Osborn T. R. and W. R. Crawford (1980) An airfoil probe for measuring velocity fluctuations in the water. In: *Air–sea interactions: instruments and methods*, F. W. Dobson, L. Hasse and R. Davis, editors, Plenum, New York, pp. 369–386.

Osborn T. R. and R. G. Lueck (1985) Turbulence measurements from a towed body. *Journal of Atmospheric and Oceanic Technology*, **2**, 517–527.

Peters H., M. C. Gregg and J. M. Toole (1988) On the parameterization of equatorial turbulence. *Journal of Geophysical Research*, **93**, 1199–1218.

Riley G. A. (1982) Biological processes on Georges Bank. In: *Georges Bank, past, present and future of a marine environment*, G. C. McLeod and J. H. Prescott, editors, Westview Press, Boulder, CO, pp. 61–76.

Shay T. J. and M. C. Gregg (1986) Convectively driven turbulent mixing in the upper ocean. *Journal of Physical Oceanography*, **16**, 1777–1798.

Stillinger D. C., K. N. Helland and C. W. Van Atta (1983) Experiments on the transition of homogeneous turbulence to internal waves in a salt-stratified fluid. *Journal of Fluid Mechanics*, **131**, 91–122.

Turner J. S. (1973) *Buoyancy effects in fluids*, Cambridge University Press, Cambridge, U.K., 367 pp.

Yamazaki H. and T. Osborn (1993) Dissipation estimates for stratified turbulence. *Journal of Physical Oceanography*, **95**, 9739–9744.